Acta Cryst C STRUCTURAL CHEMISTRY
ISSN 2053-2296

Synthesis, experimental and *in silico* studies of *N*-fluorenylmethoxycarbonyl-*O*-*tert*-butyl-*N*-methyltyrosine, coupled with CSD data: a survey of interactions in the crystal structures of Fmoc–amino acids

Joanna Bojarska,[a]* Milan Remko,[b] Izabela D. Madura,[c] Krzysztof Kaczmarek,[d] Janusz Zabrocki[d] and Wojciech M. Wolf[a]

[a]Institute of General and Ecological Chemistry, Lodz University of Technology, Faculty of Chemistry, Żeromskiego 116, Lodz 90-924, Poland, [b]Remedika, Sustekova 1, 85104 Bratislava, Slovakia, [c]Warsaw University of Technology, Faculty of Chemistry, Noakowskiego 3, 00-664 Warszawa, Poland, and [d]Institute of Organic Chemistry, Lodz University of Technology, Faculty of Chemistry, Żeromskiego 116, Lodz 90-924, Poland. *Correspondence e-mail: joanna.bojarska@p.lodz.pl

Received 30 November 2019
Accepted 3 March 2020

Edited by H. Shepherd, University of Canterbury, England

Keywords: Fmoc amino acids; supramolecular synthon; tecton; DFT; Hirshfeld surface; electrostatic molecular potential; SC-XRD; energy framework; crystal structure.

CCDC reference: 1951365

Supporting information: this article has supporting information at journals.iucr.org/c

Recently, fluorenylmethoxycarbonyl (Fmoc) amino acids (*e.g.* Fmoc–tyrosine or Fmoc–phenylalanine) have attracted growing interest in biomedical research and industry, with special emphasis directed towards the design and development of novel effective hydrogelators, biomaterials or therapeutics. With this in mind, a systematic knowledge of the structural and supramolecular features in recognition of those properties is essential. This work is the first comprehensive summary of noncovalent interactions combined with a library of supramolecular synthon patterns in all crystal structures of amino acids with the Fmoc moiety reported so far. Moreover, a new Fmoc-protected amino acid, namely, 2-{[(9*H*-fluoren-9-ylmethoxy)carbonyl](methyl)amino}-3-{4-[(2-hydroxypropan-2-yl)oxy]phenyl}propanoic acid or *N*-fluorenylmethoxycarbonyl-*O*-*tert*-butyl-*N*-methyltyrosine, Fmoc-*N*-Me-Tyr(*t*-Bu)-OH, $C_{29}H_{31}NO_5$, was successfully synthesized and the structure of its unsolvated form was determined by single-crystal X-ray diffraction. The structural, conformational and energy landscape was investigated in detail by combined experimental and *in silico* approaches, and further compared to *N*-Fmoc-phenylalanine [Draper *et al.* (2015). *CrystEngComm*, **42**, 8047–8057]. Geometries were optimized by the density functional theory (DFT) method either *in vacuo* or *in solutio*. The polarizable conductor calculation model was exploited for the evaluation of the hydration effect. Hirshfeld surface analysis revealed that H···H, C···H/H···C and O···H/H···O interactions constitute the major contributions to the total Hirshfeld surface area in all the investigated systems. The molecular electrostatic potentials mapped over the surfaces identified the electrostatic complementarities in the crystal packing. The prediction of weak hydrogen-bonded patterns *via Full Interaction Maps* was computed. Supramolecular motifs formed *via* C—H···O, C—H···π, (fluorenyl)C—H···Cl(I), C—Br···π(fluorenyl) and C—I···π(fluorenyl) interactions are observed. Basic synthons, in combination with the *Long-Range Synthon Aufbau Modules*, further supported by energy-framework calculations, are discussed. Furthermore, the relevance of Fmoc-based supramolecular hydrogen-bonding patterns in biocomplexes are emphasized, for the first time.

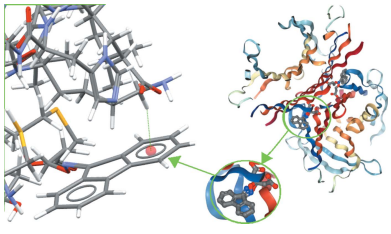

1. Introduction

Amino acids (AAs) are essential building blocks for living organisms which carry the prime important structural information for an understanding of biological processes. AAs and short peptides are attracting increasing attention due to their numerous advantages (Zhou *et al.*, 2017; Bojarska *et al.*, 2018,

2019*a*), namely, large chemical diversity, simple administration as medicines and superior properties, such as good stability, robustness, biocompatibility, natural availability, low toxicity, high specificity in protein binding, selective modes of action and low side effects. Their production and chemical modifications are relatively easy. Recently, peptide-based therapeutics have shown a significant renaissance with respect to medical applications. The size and shape of oligopeptides can be modified to fill the gap between conventional small molecular drugs and proteins. Peptides override the shortcomings of small molecules and can be more easily optimized for recognition of particular targets (Farhadi & Hashemian, 2018). Short peptides can easily penetrate cell membranes in either direction (Guidotti *et al.*, 2017). They have become a unique class of pharmaceuticals with distinct biotherapeutic features (Lee *et al.*, 2019). The progress in the field is reflected by the growing number of peptide drugs approved and the development of cosmeceuticals, which deliver a biological activity in support of cosmetic action (Henninot *et al.*, 2018; Pai *et al.*, 2017; Bojarska *et al.*, 2018, 2019*a*,*b*). Short peptides play a crucial role in the metabolism of living cells, with special emphasis directed towards antioxidant, antibacterial, antitumour, anti-aging and anti-inflammatory activities. Additionally, their involvement in the regulation of the neuro-immuno-endocrine system cannot be neglected (Sánchez & Vázquez, 2017; Kraskovskaya *et al.*, 2017; Zamorskii *et al.*, 2017; Khavinson *et al.*, 2017). In particular, modified AAs and ultra-short peptides have broad applications for either the biomedical industry or research, namely, anticancer therapy, immunology, tissue engineering, the design of modern drugs delivery systems, catalysis or biofunctional supramolecular materials (Zhou *et al.*, 2017; Diaferia *et al.*, 2019). AAs and dipeptides protected at the N-terminus with large aromatic groups, like fluorenylmethoxycarbonyl (Fmoc), are used as *inter alia* effective low-molecular-weight hydrogelators (especially Fmoc–tyrosine and Fmoc–phenylalanine). The latter are used as molecular biomaterials (Du *et al.*, 2015) and applied in the control of drug release (Mahler *et al.*, 2006), in tissue engineering and cell culturing (Jayawarna *et al.*, 2009), sensing, encapsulation or as electronic materials (Fleming & Ulijn, 2014; Ryan & Nilsson, 2012; Adams, 2011; Liebmann *et al.*, 2007; Ikeda *et al.*, 2014; Sutton *et al.*, 2009; Liang *et al.*, 2009; Nalluri *et al.*, 2014). The Fmoc moiety is an important component of several drug molecules, such as an antibiotic (cicloprofen or ledipasvir) inhibitor NS5A protein used in the treatment of viral hepatitis. Fmoc–AAs have found applications in therapies for Alzheimer's disease and other neurodegenerative symptoms leading to memory loss and cognitive impairment. The former was initially observed, at the beginning of the 20th century, by the German psychiatrist Alois Alzheimer, as a novel form of dementia. Remarkably, it is one of the leading causes of death in the world and, according to the World Health Organization, it contributes to over two-thirds of dementia cases worldwide (World Health Organization, 2019; Kasim *et al.*, 2019). Therefore, there is an obvious need for more selective inhibitors involved in neuronal signal transduction. This issue is currently being studied intensely. The Fmoc moiety exhibits a structural affinity for the active sites of cholinesterases (acetylcholinesterase and butyrylcholinesterase). Therefore, Fmoc–AAs are attractive scaffolds for further development (Gonzalez *et al.*, 2016; Ramirez *et al.*, 2018; Pingul *et al.*, 2019).

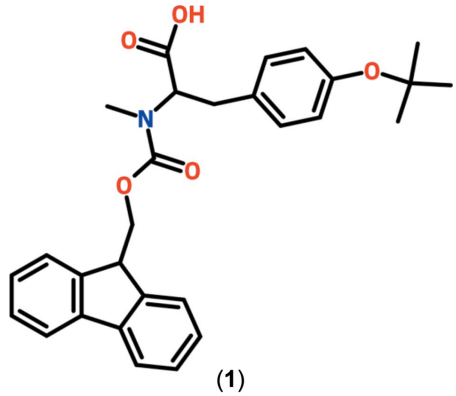

(**1**)

Scheme 1

Although several reports concerning Fmoc–AAs have appeared, the supramolecular aspects have not been thoroughly discussed so far. This study attempts to fill this gap, being, according to the best of our knowledge, the first comprehensive work classifying interactions involved in the formation of supramolecular synthon patterns related to Fmoc–AAs. In the first part, we focus on the synthesis and detailed characterization of the molecular and supramolecular structure of a novel unsolvated form of an Fmoc–AA, namely *N*-fluorenylmethoxycarbonyl-*O*-*tert*-butyl-*N*-methyltyrosine, (**1**) (Scheme 1). We compare it with the previously reported derivative *N*-(fluorenylmethoxycarbonyl)phenylalanine (CSD refocde OGIXOT; Draper *et al.*, 2015). Topological analysis, basic supramolecular hydrogen-bonding patterns and large synthons, so called *Long-Range Synthon Aufbau Modules* (Ganguly & Desiraju, 2010), and energy frameworks are described. Molecular geometries, optimized in either the gas phase or the solvated state by density functional theory (DFT) methods, are compared. In the second section, a comprehensive comparative analysis and a hierarchy of the intermolecular interactions in all known relevant Fmoc–AA structures, as retrieved from the Cambridge Structural Database (CSD; Version 5.40, update February 2019; Groom *et al.*, 2016) (see Schemes S1 and S2 in the supporting information), are considered. Generally, we divided privileged Fmoc–Tyr/Phe derivatives into the following groups: **A** – containing a substituent O atom in the phenyl ring [(**1**), CAMLEK (Fichman *et al.*, 2016), INEJEQ (Clegg & Elsegood, 2003), OGIYAG (Draper *et al.*, 2015) and OGOGIA (Young & Kiessling, 2002)]; **B** – without substituents in the phenyl ring [OGIXOT, EKEWUM (Clegg & Elsegood, 2003), NUBPEH (Raeburn *et al.*, 2015), OGIXUZ (Draper *et al.*, 2015) and VERXUO (Rajbhandary *et al.*, 2018)]; **C** – with an additional chain as substituent in the molecular backbone [MOXSUP (Scroggs *et al.*, 2015) and DULLAZ (Wang *et al.*, 2015)]; **D** – containing other substituents in the phenyl ring [UQIYUQ, UQOGUE (Liyanage & Nilsson, 2016) and WATSIU01 (Stefanowicz *et al.*, 2006)]; **E** – including halogen atoms

Table 1
Experimental details.

Crystal data	
Chemical formula	$C_{29}H_{31}NO_5$
M_r	473.55
Crystal system, space group	Orthorhombic, $P2_12_12_1$
Temperature (K)	296
a, b, c (Å)	6.4917 (3), 17.5357 (7), 22.2418 (8)
V (Å^3)	2531.93 (18)
Z	4
Radiation type	Mo $K\alpha$
μ (mm^{-1})	0.09
Crystal size (mm)	0.60 × 0.25 × 0.15
Data collection	
Diffractometer	Siemens P3
Absorption correction	Multi-scan (*SADABS*; Sheldrick, 2008)
T_{min}, T_{max}	0.872, 0.992
No. of measured, independent and observed [$I > 2\sigma(I)$] reflections	58330, 5823, 5543
R_{int}	0.022
(sin $\theta/\lambda)_{max}$ (Å^{-1})	0.649
Refinement	
$R[F^2 > 2\sigma(F^2)]$, $wR(F^2)$, S	0.032, 0.091, 0.99
No. of reflections	5823
No. of parameters	396
H-atom treatment	H atoms treated by a mixture of independent and constrained refinement
$\Delta\rho_{max}$, $\Delta\rho_{min}$ (e Å^{-3})	0.15, −0.16
Absolute structure	Flack x determined using 2313 quotients $[(I^+) - (I^-)]/[(I^+) + (I^-)]$ (Parsons & Flack, 2004)
Absolute structure parameter	0.19 (14)

Computer programs: *XSCANS* (Siemens, 1996), *SHELXT* (Sheldrick, 2015*a*), *SHELXL2014* (Sheldrick, 2015*b*), *Mercury* (Macrae *et al.*, 2020) and *PLATON* (Spek, 2020).

(XATJAG, XATJEK, XATKEL and XATKIP; Pizzi *et al.*, 2017). Notably, OGOGIA, INEJEQ and EKEWUM possess a modified –COOH group. Apart from the mentioned compounds, other derivatives of Fmoc–AAs are as follows: alanine [ADAGUK (Xing *et al.*, 2017), CUWKIO01 (Al-Mahamad *et al.*, 2017) and CUWKOU01 (Hammarstrom *et al.*, 2013)], cysteine (EJEWUL; Liu *et al.*, 2002), glycine [NOVTOJ (Wu *et al.*, 2015), VERQER, VERQIV, VERQOB, VERXIC and VERXOI (Rajbhandary *et al.*, 2018), and XAVYIE (Rudat *et al.*, 2011)], isoleucine (QOFHID; Yamada *et al.*, 2008), leucine (BIZXUE; Yamada *et al.*, 2008), ornithine (EXOFAY; Mazur *et al.*, 2002), serine [ADAGOE (Xing *et al.*, 2017) and MOHCIW (Yamada *et al.*, 2008)] and tryptophan (DIZNIK; Blaser *et al.*, 2008).

The effect of the substituent in the phenyl ring and modification of the –COOH group in the Fmoc–AA core is discussed to acquire a deeper understanding of the observed differences in the supramolecular frameworks and topologies among particular types of AAs. Visualization and quantification of the interactions based on Hirshfeld surface analyses, including electrostatic potential maps, is presented. Moreover, the probability of synthons formed by weak nonbonding interactions (involving the π-system of the Fmoc moiety) was computed and the interaction landscape of the molecules was generated *via* the *Full Interaction Maps* software. A library of the structure-determining supramolecular hydrogen-bonding patterns for different types of Fmoc–AAs is provided (Bernstein *et al.*, 1995; Etter *et al.*, 1990, 1991; Desiraju, 1989, 1995; Steiner, 2002). A great deal of attention has been focused on the use of the large planar rigid aromatic Fmoc group in a branch of crystal engineering with the emphasis on the presence of Fmoc-based supramolecular hydrogen-bonding patterns in biocomplexes (PDB, 2019 release; Berman *et al.*, 2000). We believe that this study could provide a better holistic insight into the supramolecular landscape of Fmoc–AAs as biologically active molecular targets towards the design and development of innovative drugs and hydrogels, better inhibitors of neurodegenerative diseases, other smart supramolecular biofunctional materials and so on.

2. Experimental

2.1. Materials

The reagents used to prepare the title compound were commercially available (Sigma–Aldrich) and were used without further purification or drying.

2.2. Synthesis

Fmoc-*N*-Me-Tyr(t-Bu)-OH, (**1**), was synthesized from *Z*-Tyr(t-Bu)-OH·DCHA (DCHA is dicyclohexylamine; IRIS, Germany) according to Scheme 2.

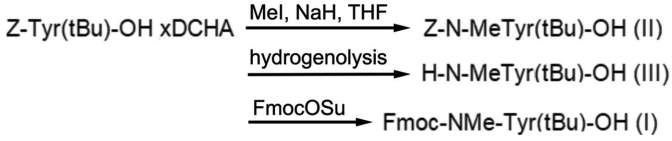

Scheme 2

We did not release the acid from its salt prior to alkylation because free *Z*-Tyr(t-Bu)-OH is not a crystalline substance, which makes its handling very difficult, particularly on a larger scale. DCHA, as present in the reaction mixture, did not harm the reaction itself, but required one more equivalent of reagents to be added. The tertiary amine obtained as a side product (dicyclohexylmethylamine) is easily separable from the expected product. The crude *N*-methylated amino acid (**II**) derivative was then hydrogenated over 10% Pd/C (Aldrich) as a catalyst to remove the *Z*-(benzyloxycarbonyl) protecting group from nitrogen, leaving the *tert*-butyl ether group untouched. Finally, the Fmoc nitrogen-protecting group was introduced to (**III**) with the aid of FmocOSu (Su = succinimidyl; IRIS, Germany) in a dioxane–water mixture in the presence of sodium bicarbonate as base. The crude product was recrystallized from a dioxane–ethyl acetate mixture, giving white crystals of the final compound suitable for X-ray analysis.

2.3. Crystallization, single-crystal X-ray structure determination and refinement

Good-quality plate-shaped single crystals suitable for X-ray diffraction (SC-XRD) analysis were grown by vapour diffu-

Table 2
Crystal data of other known Fmoc–Tyr/Phe derivatives.

CSD code	CAMLEK	OGOGIA	OGIYAG	INEJEQ	OGIXOT	VERXUO	OGIXUZ	EKEWUM	NUBPEH
	Group **A**				Group **B**				
Structural formula	$C_{24}H_{21}NO_6$	$C_{26}H_{24}N_4O_5$	$C_{24}H_{21}NO_5\cdot H_2O$	$C_{30}H_{33}NO_6\cdot 1.5CHCl_3$	$C_{24}H_{21}NO_4$	$C_{24}H_{21}NO_4\cdot C_2H_6OS$	$C_{24}H_{21}NO_4\cdot 2CH_4O$	$C_{24}H_{22}N_2O_4$	$C_{33}H_{30}N_2O_5\cdot 0.88H_2O$
Crystal system	monoclinic	orthorhom.	monoclinic	monoclinic	monoclinic	triclinic	monoclinic	orthorhom.	monoclinic
Space group	$P2_1$	$P2_12_12_1$	$C2$	$P2_1$	$P2_1$	$P1$	$P2_1$	$P2_12_12_1$	$C2$
Density (Mg m^{-3})	1.384	1.325	1.346	1.408	1.344	1.361	1.288	1.371	1.269
a (Å)	12.673 (3)	5.019 (0)	18.640 (16)	12.142 (1)	13.157 (1)	5.015 (4)	13.076 (6)	5.524 (4)	52.270 (50)
b (Å)	5.687 (1)	19.203 (1)	5.992 (5)	5.378 (0)	4.908 (0)	13.125 (10)	4.887 (2)	14.988 (11)	5.010 (6)
c (Å)	15.101 (4)	24.566 (2)	18.841 (15)	24.926 (2)	16.124 (1)	17.419 (14)	18.998 (9)	23.557 (18)	22.830 (30)
α (°)	90.00	90.00	90.00	90.00	90.00	96.47 (1)	90.00	90.00	90.00
β (°)	112.37 (1)	90.00	98.83 (1)	98.44 (1)	113.14 (0)	94.35 (1)	106.42 (1)	90.00	105.49 (3)
γ (°)	90.00	90.00	90.00	90.00	90.00	90.12 (1)	90.00	90.00	90.00
$R1$ (%) [$I > 2\sigma(I)$]	5.35	6.67	3.70	5.31	4.55	8.71	12.69	5.17	10.27
Temperature (K)	100	173	100	160	100	100	100	173	100
KPI* (%)	69.7	67.4	69.4	55.8	70.1	71.5	68.8	71.3	67.1

CSD code	MOXSUP	DULLAZ	WATSIU01	UQOGUE	UQIYUQ	XATKEL	XATJAG	XATJEK	XATKIP
	Group **C**		Group **D**			Group **E**			
Structural formula	$C_{31}H_{27}NO_4\cdot 0.33C_6H_{14}$	$C_{28}H_{29}NO_4$	$C_{24}H_{21}N_3O_6\cdot 2CH_2Cl_2$	$0.7C_{25}H_{20}N_2O_4\cdot 0.3C_{24}H_{20}N_2O_6$	$C_{25}H_{23}NO_4$	$C_{24}H_{20}INO_4\cdot 0.333H_2O$	$C_{24}H_{20}BrNO_4\cdot 0.3H_2O$	$C_{24}H_{20}ClO_4$	$C_{24}H_{20}FO_4\cdot C_2H_6OS$
Crystal system	orthorhom.	monoclinic	monoclinic	orthorhom.	orthorhom.	hexagonal	hexagonal	monoclinic	orthorhom.
Space group	$Pbca$	$P2_1$	$P2_1$	$P2_12_12_1$	$P2_12_12_1$	$P6_3$	$P6_3$	$P2_1$	$P2_12_12_1$
Density (Mg m^{-3})	1.263	1.246	1.415	1.374	1.339	1.654	1.520	1.357	1.361
a (Å)	5.379 (1)	5.444 (3)	12.362 (3)	5.747 (3)	5.675 (0)	26.878 (4)	26.744 (4)	13.168 (3)	4.920 (1)
b (Å)	25.977 (4)	38.160 (20)	10.489 (3)	15.850 (7)	15.661 (1)	26.878 (4)	26.744 (4)	4.839 (1)	13.034 (3)
c (Å)	38.081 (6)	11.382 (6)	22.958 (4)	22.201 (10)	22.411 (3)	4.999 (1)	4.997 (0)	17.400 (4)	36.789 (7)
α (°)	90.00	90.00	90.00	90.00	90.00	90.00	90.00	90.00	90.00
β (°)	90.00	90.13 (3)	103.17 (3)	90.00	90.00	90.00	90.00	111.41 (3)	90.00
γ (°)	90.00	90.00	90.00	90.00	90.00	120.00	120.00	90.00	90.00
$R1$ (%) [$I > 2\sigma(I)$]	5.60	9.99	6.14	6.01	5.44	7.33	6.91	6.65	11.5
Temperature (K)	90	110	100	100	100	100	100	100	100
KPI* (%)	62.9	67.2	66.9	71.6	70.6	71	71	67.8	70.9

Note: (*) Kitaigorodsky's packing index.

sion over a period of a few weeks. All nonmethyl H atoms were found in a difference Fourier map and refined isotropically. Methyl H atoms were placed in calculated positions based on local difference density, and refined as riders with the methyl groups allowed to rotate but not tilt; U_{iso}(H) values were set at 1.2U_{eq}(C) for the methyl groups.

Crystal data, data collection and structure refinement details for (**1**) are summarized in Table 1. In addition, crystallographic information on the sole Fmoc–Tyr/Phe derivative, which was reported in the CSD, is presented in Table 2. Molecular plots, packing diagrams and geometrical calculations were prepared using the *Mercury* (Macrae *et al.*, 2020) and *PLATON* (Spek, 2020) programs.

2.4. Theoretical calculations

2.4.1. DFT study. Density functional theory (DFT) calculations were performed using the *GAUSSIAN09* package (Frisch *et al.*, 2011). The geometry of *N*-fluorenylmethoxycarbonyl-*O*-*tert*-butyl-*N*-methyltyrosine, (**1**), obtained from the X-ray analysis, was completely optimized. For calculations of the stable conformers in both the gas phase and the solvated state, DFT calculations (Parr & Wang, 1994; Neumann *et al.*, 1996; Bickelhaupt & Baerends, 2000) at the B3LYP level of theory (Becke, 1988, 1993; Lee *et al.*, 1988) and the polarized triple-ζ 6-311++G(d,p) basis set were used. The polarizable conductor calculation model (CPCM) (Klamt & Schüürmann, 1993; Barone & Cossi, 1998; Cossi *et al.*, 2003) was exploited for the evaluation of the hydration effect on the structure of (**1**). To evaluate the effect of substitution (phenyl-*O*-*tert*-butyl and *N*-methyl) on the geometry of the central amino acid scaffold, we also examined the structure of *N*-Fmoc-phenylalanine (OGIXOT; Draper *et al.*, 2015).

2.4.2. Hirshfeld surface analysis. For the Hirshfeld surface (HS) analysis, the *CrystalExplorer* program was used (Version 17.5; Turner *et al.*, 2017; Wolff *et al.*, 2012). Intermolecular interactions were analyzed qualitatively and quantitatively *via* 3D HSs and 2D (two-dimensional) fingerprint plots (FPs), respectively. Molecular geometries were as determined by X-ray analysis (based on the CIF files), with H atoms adjusted to their neutron positions. The bond lengths of all H atoms were normalized to the standard neutron diffraction values (Allen *et al.*, 1987). HSs (Spackman & McKinnon, 2002) account for the electron distributions calculated for spherical atoms (Spackman & Byrom, 1997; McKinnon *et al.*, 1998, 2007). They were generated following normalized contact distances d_{norm}, shape index and curvedness. The FPs, defined as scattergrams of internal distances (d_i) *versus* external distances (d_e) for particular HS points, were also generated (Rohl *et al.*, 2008). A quantitative decomposition of the atom-

to-surface contacts was calculated as a percentage of points within the HS for pairs of atoms within the predefined shell (d_i, d_e). Furthermore, the electrostatic molecular potentials (ESPs) mapped on the HS (Spackman *et al.*, 2008) for all Fmoc–AA derivatives were calculated. *Ab initio* wave functions were computed for a single molecule using the *TONTO* approach (Jayatilaka & Grimwood, 2003) at the HF/6-311++G(3df,2pd) level.

2.5. Database survey

Details of the CSD analysis (Version 5.40, update February 2019; Groom *et al.*, 2016) are presented in Scheme S1 in the supporting information. The search yielded 35 structures, namely, 18 structures of Fmoc-based tyrosine/phenylalanine, seven of Fmoc–glycine, three of Fmoc–alanine, two of Fmoc–serine, one of Fmoc–cysteine, one of Fmoc–isoleucine, one of Fmoc–leucine, one of Fmoc–ornithine and one of Fmoc–tryptophan (Tables S1–S3 in the supporting information). The structure of OGIXOT (Draper *et al.*, 2015) is the simplest AA among those analyzed and the most similar to (**1**). It crystallizes in the monoclinic space group $P2_1$, with one independent molecule in the asymmetric unit. Furthermore, the Protein Data Bank (PDB) was searched for 3D macromolecular crystal structures of biocomplexes with the fluorene moiety and resulted in 40 hits.

3. Results and discussion

3.1. Description of the crystal and molecular structure of (1) *versus* OGIXOT

The title compound, (**1**), crystallizes in the orthorhombic noncentrosymmetric Sohnke space group $P2_12_12_1$. It contains one molecule in the asymmetric unit of the crystal lattice. The X-ray molecular structure is shown in Fig. 1.

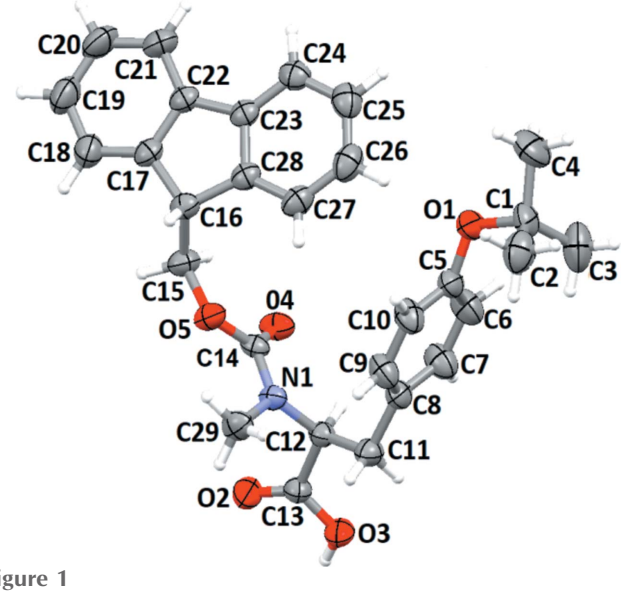

Figure 1
The molecular structure of (**1**), showing the atom-labelling scheme. Displacement ellipsoids are drawn at the 50% probability level and H atoms are shown as small spheres of arbitrary radii.

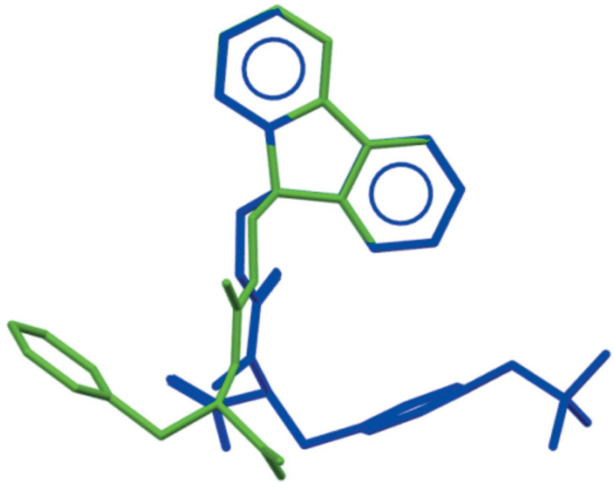

Figure 2
An overlay of the molecules of (**1**) (in blue) and OGIXOT (in green). H atoms have been omitted for clarity.

The bond lengths and angles are within normal ranges. The molecule has a substantially planar conformation. The fluorenyl group (Fmoc), *O*-substituted phenyl ring and carbamate linkage (atoms C12–C15/O5) are all essentially planar. The *tert*-butylphenyl substituent is *gauche* with respect to the carbamate group (−62°) and *anti* to the carboxyl group (170°). The *tert*-butyl group lies nearly perpendicular to the plane of the phenyl ring. The N atom is sp^2-hybridized and adopts a nearly planar configuration, with the sum of all three relevant valence angles approaching 360°. Fig. 2 depicts a superposition of (**1**) and OGIXOT (Draper *et al.*, 2015). In both compounds, the amide bond is in a *trans* conformation. Nevertheless, notable differences between the two structures are apparent. This is not surprising due to the long alkyl chain. The main difference is seen in the torsion angles between the phenyl-*O*-*tert*-butyl and phenyl moieties. In addition, the orientation of the C═O bonds exhibits obvious differences as well. A further superposition, including all Fmoc–Tyr/Phe derivatives, is shown in Fig. S1 in the supporting information.

3.2. DFT study

Density functional theory (DFT) calculations were used to determine the molecular structure of (**1**) in the gas phase and/or in water solution. The initial conformations used in calculations were constructed using the *GaussView* graphical interface (Nielsen & Holder, 2009). We took the relative orientations of the bulky substituents of the carbamate group from the X-ray data of the crystal structure discussed earlier. The overlay of the X-ray structure of (**1**) and the B3LYP-optimized structure of this compound are shown in Fig. 3(*a*). However, in the solid state, the molecules are immersed in an ordered environment defined by other molecules. The crystal packing forces and strong intermolecular O—H···O═C hydrogen-bond network present in the crystal structure of (**1**) impose a distinct conformational preference for this molecule when located in different environments. Thus, the largest differences in the gas phase and solid-state geometry are

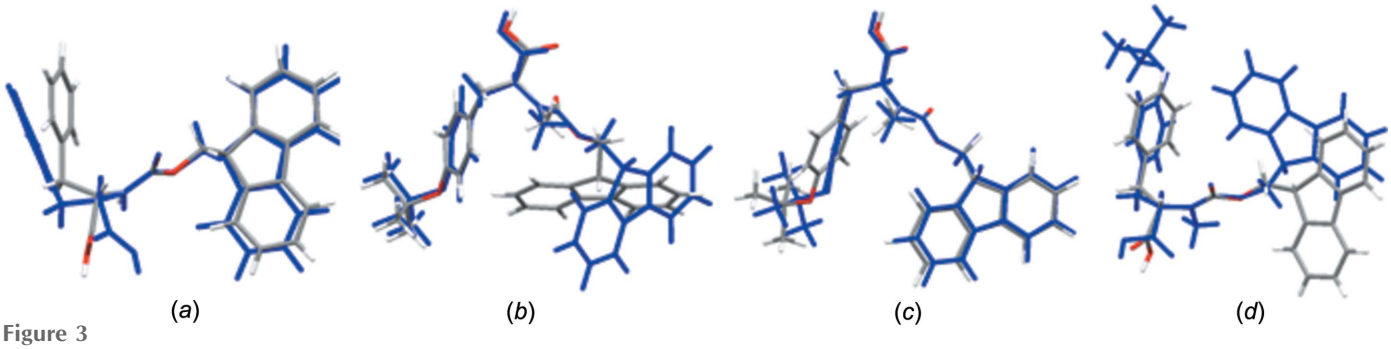

Figure 3
Superposition (with respect to the O═C—N group) of the structure of (**1**) and (*a*) B3LYP-optimized (**1**) (blue), (*b*) B3LYP-optimized solvated (**1**) (blue), (*c*) B3LYP-optimized (**1**) and B3LYP-optimized solvated (**1**) (blue), and (*d*) B3LYP-optimized (**1**) (blue) and OGIXOT.

observed for the torsion angles mainly. The carbamate group is almost planar in all environments (torsion angle C15—O5—C14—N1). The molecular structure of the solid-state conformer is stabilized *via* an intramolecular interaction between the polar C26—H hydrogen of the phenyl ring and the O atom of the neighbouring *tert*-butylphenyl substituent (C26—H···O1 = 2.4 Å). By the lack of this interaction in the gas phase and/or water solution, the bulky 9-fluorenylmethyl group is rotated away from the *tert*-butylphenyl substituent of the carbamate group, making a C14—O5—C15—C16 torsion angle of about 175°, with a large deviation of about 50° compared to the solid-state structure (Table 3). A highly extended structure is observed in water solution, with a large interatomic C26—H···O1 distance of 6.5907 Å. The optimized structures are shown in Fig. 3, and Fig. S2 in the supporting information. As regards the unsubstituted derivative OGIXOT, in the absence of the C26—H···O1 interaction in the isolated molecule of (**1**), the equilibrium geometry of

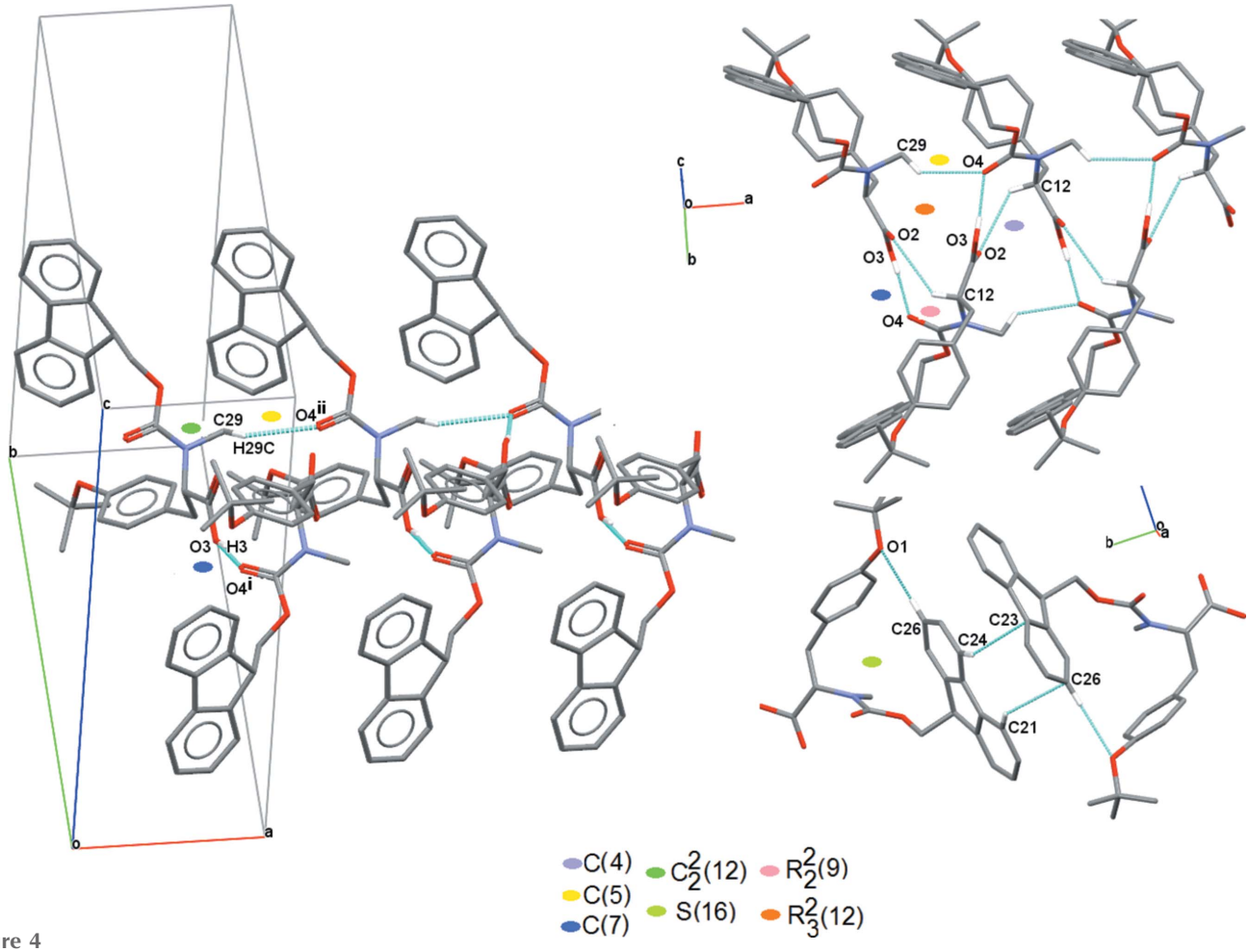

Figure 4
The crystal packing of (**1**), showing the intermolecular hydrogen bonds involved in the formation of supramolecular hydrogen-bond patterns [symmetry codes: (i) $x+\frac{1}{2}, -y-\frac{1}{2}, -z+2$; (ii) $x+1, y, z$]. H atoms not involved in hydrogen bonds have been omitted for clarity.

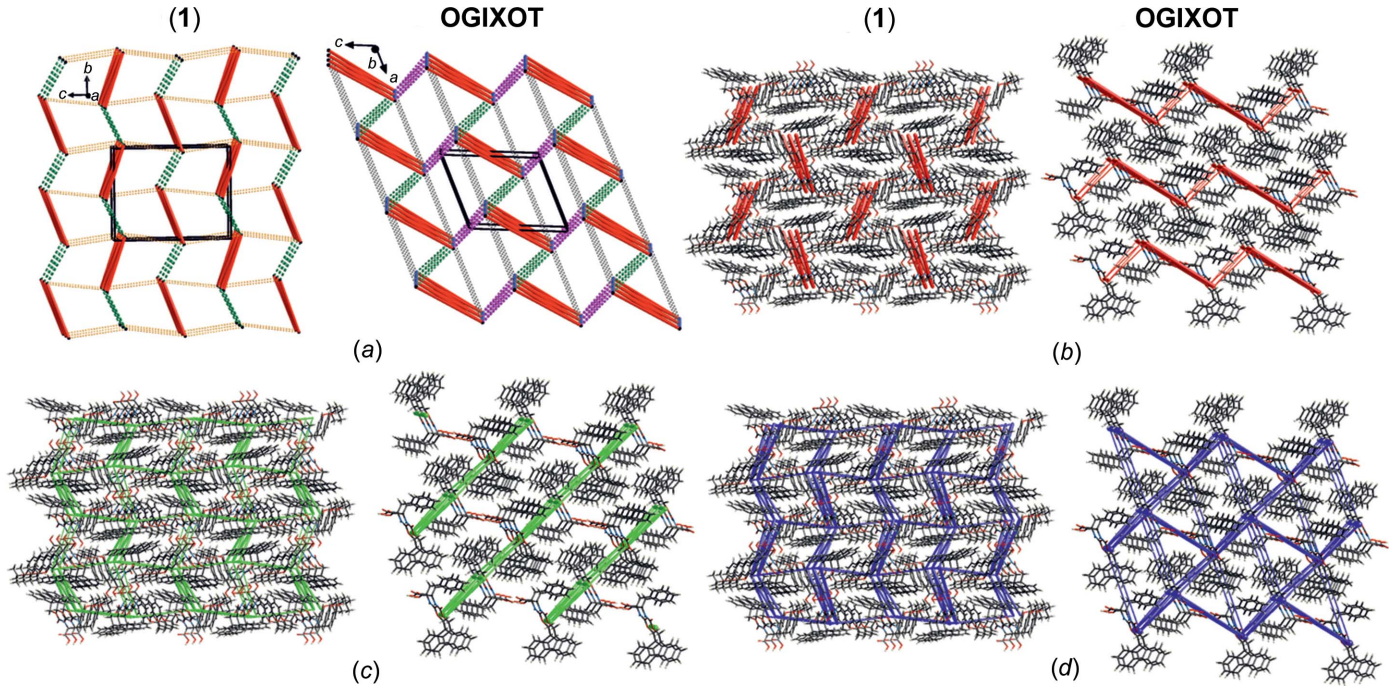

Figure 5
(*a*) Large synthons (solid lines) for (**1**) and OGIXOT. Dotted green lines indicate C—H···π interactions formed between Fmoc fragments, pink lines represent interactions between phenyl rings, orange lines in (**1**) correspond to other weak interactions along the [001] direction and grey dotted lines in OGIXOT represent weak phenyl–Fmoc contacts. Energy frameworks in (**1**) (viewed along the *a* axis) and OGIXOT (viewed along the *b* axis). (*b*) Red, (*c*) green and (*d*) blue tubes are given with the same size and represent electrostatic, dispersion and total energy contributions, respectively.

OGIXOT represents a more extended structure minimizing the repulsive forces between both hydrophobic side groups and resulting in different values of the torsion angles C12—C11—C8—C7 and N1—C12—C13—O2 (Table 3). In the solid state, (**1**) crystallized as needle-shaped crystals and crystal packing forces stabilize adjacent molecules *via* intermolecular N—H···O(=C) hydrogen bonds between the carboxylic acid and amide groups of the phenylananine moiety. In the absence of this hydrogen-bonding network, in the isolated molecules, the overall shape of the equilibrium geometry results in more extended structures (torsion angles C12—C11—C8—C7 and N1—C12—C13—O2). The solvent effect (water) does not change the equilibrium structure of the isolated molecule appreciably (Fig. S2 in the supporting information).

Table 3
Experimental and theoretically optimized relevant torsion angles (°) of (**1**) and OGIXOT.

	(**1**)			OGIXOT		
Parameter	X-ray	DFT	DFT-CPCM	X-ray	DFT	DFT-CPCM
	(**1**)			OGIXOT		
O5—C15—C16—C17	74.59 (15)	72.92	71.01	−71.88	−71.17	−69.93
C14—O5—C15—C16	−125.55 (16)	−174.18	176.94	175.11	−179.31	176.28
N1—C12—C11—C8	−62.60 (18)	−55.27	−63.08	−66.60	−64.17	−63.88
C12—C11—C8—C7	−75.24 (2)	−47.38	−74.18	−94.58	−75.63	−74.21
N1—C12—C13—O2	18.32 (2)	−8.10	1.41	134.27	167.89	164.11
C15—O5—C14—N1	−175.97 (14)	−177.07	−177.97	175.03	178.24	179.18
C26—H···O1 (Å)	2.40648 (16)	4.9518	6.5907	–	–	–

3.3. Supramolecular features

3.3.1. Supramolecular architecture of (1). The title crystal is characterized by classical and nonclassical intra- and intermolecular hydrogen bonds influenced by various functional groups present in the structure (–C=O, –COOH, –O–, –NCH_3 and -*tert*-butyl). The supramolecular assembly is stabilized by strong O—H···O(=C) hydrogen bonds between the carbamate and carboxylic acid groups, supported by weak C—H···O(=C) hydrogen-bonding interactions between the carbamate and methyl groups. Atoms O2, O5 and N1 do not participate in hydrogen bonds. Hydrogen-bond geometry data for (**1**) are summarized in Table 4. Following the hydrogen-bond supramolecular synthon pattern approach, atoms O3 and C29 are involved in hydrogen-bonding interactions leading to the creation of undulating seven-membered chains, along the *ac* plane, *via* (carboxyl)O3—H3···O4^{i}(carbonyl-Fmoc) hydrogen bonding and five-membered chains, along the short *a* axis, through (methyl)C29—H29*C*···O4^{ii}(carbonyl-Fmoc) interactions between the planar and rigid aromatic Fmoc and phenyl moieties, encoded as *C*(7) and *C*(5) graph-set motifs, respectively (Etter *et al.*, 1990; Bernstein *et al.*, 1995). Interplay of both interactions leads to an elongation of the supramolecular chain, *i.e.* $C_2^2(12)$. Additionally, other supramolecular hydrogen-bonding patterns, *i.e.* rings (*R*), intramolecular rings (*S*) or groups (*D*), are observed. Remarkably, the fluorenyl moiety is involved in the formation

Table 4
Hydrogen-bond geometry (Å, °).

D—H···A	D—H	H···A	D···A	D—H···A
O3—H3···O4^{i}	0.91	1.77	2.666 (1)	168
C29—H29C···O4^{ii}	0.96	2.50	3.240 (2)	134
C15—H151···O4	0.97	2.18	2.687 (2)	111
C26—H261···O1	0.96	2.41	3.369 (2)	178

Symmetry codes: (i) $x+\frac{1}{2}, -y-\frac{1}{2}, -z+2$; (ii) $x+1, y, z$.

of an (Fmoc)C26—H261···O1(*O-tert*-butyl) interaction, leading to an intramolecular large $S(16)$ graph-set motif. Overall, the crystal structure of (**1**) represents a well-developed 3D hydrogen-bond network (Fig. 4).

3.3.2. Supramolecular synthon patterns in the supramolecular assembly of (1) in relation to other Fmoc–Tyr/Phe AAs: comparative analysis of basic synthons and LSAMs *versus* energy frameworks. The crystal packing of (**1**) and OGIXOT is shown in Fig. S3 in the supporting information. Hydrogen-bond geometry data for OGIXOT augmented by 18 structures with Fmoc–Tyr/Phe moieties derived from the CSD are summarized in Table S4 of the supporting information. In OGIXOT, O—H···O, C—H···O or N—H···O hydrogen bonds link molecules together in the crystal lattice. N1—H8···O2 hydrogen bonds are involved in the formation of supramolecular $C(4)$ chains, while, in combination with C21—H16···O1 and O3—H1···O4, they yield $C_2^2(14)$ and $C_2^2(12)$ chains, respectively. These linear structures are linked together by pivotal $R_3^3(16)$ rings. Moreover, aromatic systems (either fluorenyl or phenyl), which act as weak hydrogen-bond acceptors, prompt face-to-face π–π stacking and edge-to-face C—H···π interactions. The latter involve methyl groups at exocyclic N atoms and Fmoc systems, finally leading to the formation of chains along the [010] axis with very similar geometries in both (**1**) and OGIXOT (see Table S5 in the supporting information). In OGIXOT, the π–π interactions between the three fused planar rings stabilize supramolecular stacks running along the [100] direction (Table S6 in the supporting information). In addition, the supramolecular landscape was analyzed using the *Long-Range Synthon Aufbau Modules* approach (Ganguly & Desiraju, 2010). In (**1**), these large synthons are zigzag chains built by O—H···O hydrogen bonds running parallel to the [100] direction. The strongest C—H···O and C—H···π weak interactions were found between molecules along the shortest base vector a, enhancing the large synthon, whereas weaker contacts link these chains into a 3D structure. A sole large synthon is surrounded by six neighbours, leading to a quasi-hexagonal packing of these one-dimensional (1D) objects. This, in turn, indicates that the relevant weak interactions are only partially directional and are of minor significance when the stability of

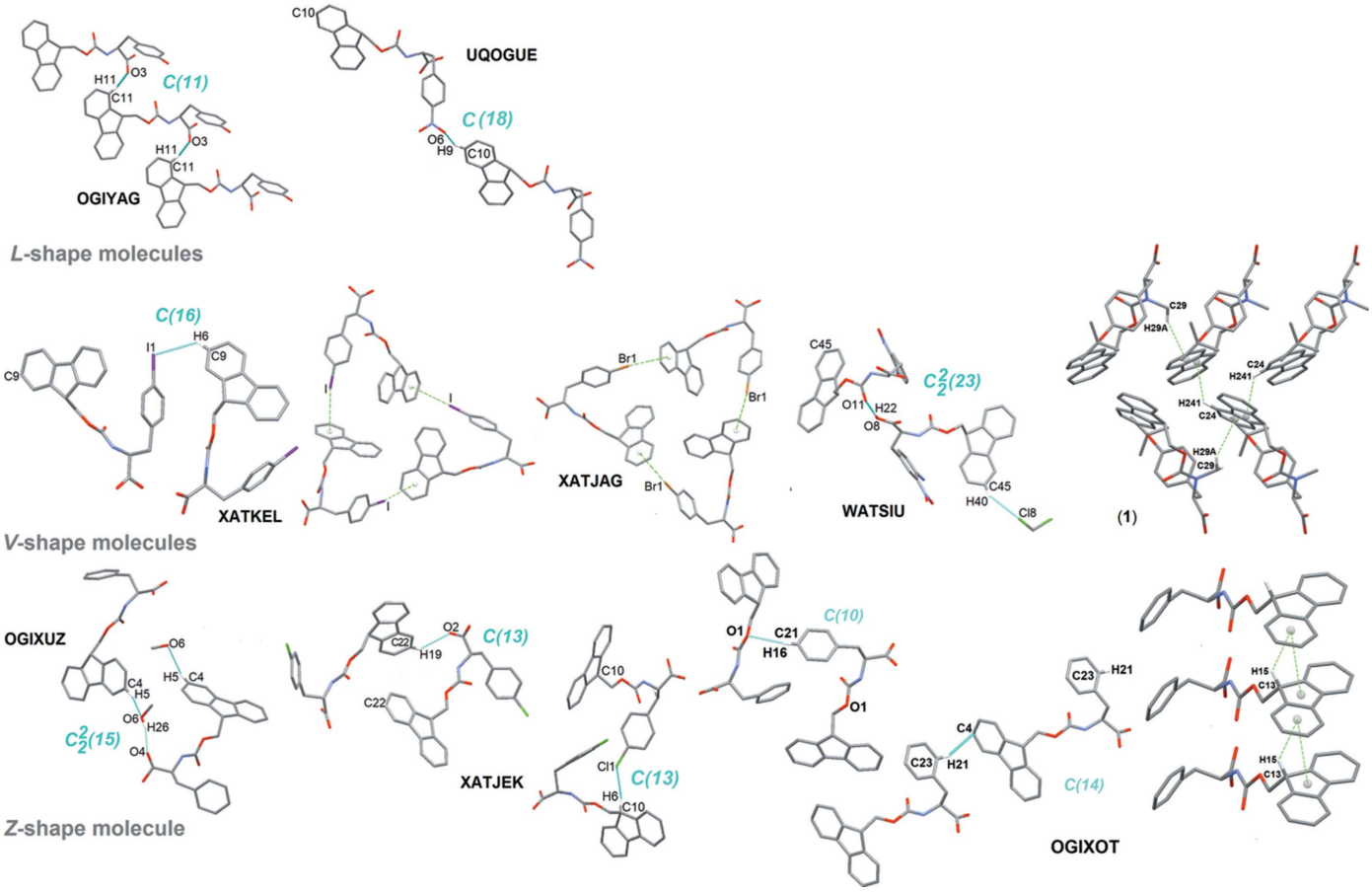

Figure 6
Selected supramolecular synthon patterns, in which fluorene is involved, found in Fmoc–AA derivatives.

Table 5
Estimated energies for the main interactions in (**1**) and OGIXOT decomposed to electrostatic (E_{ele}), polarization (E_{pol}), dispersion (E_{dis}) and repulsion (E_{rep}) components.

The total energies (E_{tot}) are the sum of the four energy components scaled appropriately for two benchmarked energy models included in the *Crystal-Explorer* (Version 1.75; Wolff *et al.*, 2012) CE_B3LYP/6-31G(d,p) and CE_HF/3-21G (data in italics).

Interaction type	R*	E_{ele}	E_{pol}	E_{dis}	E_{rep}	E_{tot}
(**1**)						
Interactions in the large synthon along the [100] direction	6.49	−10.4	−5.0	−67.2	33.7	−52.5
		−11.3	*−8.0*	*−67.2*	*24.8*	*−57.1*
O—H···O	10.65	−61.3	−15.2	−22.0	66.5	−54.2
		−66.0	*−20.8*	*−22.0*	*50.7*	*−59.5*
C—H···π (Fmoc–Fmoc)	8.89	−8.5	−2.4	−52.3	29.0	−38.4
		−9.4	*−5.2*	*−52.3*	*23.0*	*−41.4*
Secondary interactions along the [001] direction; mainly C—H···π (Fmoc–phenyl)	11.36	−6.5	−2.1	−36.2	17.4	−29.2
		−6.2	*−2.9*	*−36.2*	*12.9*	*−30.4*
	11.99	−4.0	−0.8	−23.2	7.8	−20.2
		−4.6	*−1.4*	*−23.2*	*6.1*	*−21.7*
OGIXOT						
N—H···O(peptide)	4.91	−43.2	−10.1	−81.2	66.6	−82.7
		−45.1	*−15.5*	*−81.2*	*49.9*	*−88.7*
C—H···π(phenyl–phenyl)	8.45	−14.6	−2.8	−56.0	45.5	−38.2
		−15.0	*−5.1*	*−56.0*	*35.4*	*−40.3*
O—H···O	12.44	−47.2	−12.7	−7.5	69.4	−22.9
		−53.7	*−18.7*	*−7.5*	*53.1*	*−30.7*
C—H···π(Fmoc–Fmoc)	8.60	−6.3	−1.7	−34.3	19.1	−26.0
		−6.3	*−2.5*	*−34.3*	*13.5*	*−28.0*
C—H···π(phenyl–Fmoc)	13.16	−6.2	−1.3	−16.0	9.0	−15.9
		−9.4	*−2.2*	*−16.0*	*6.9*	*−19.8*

the crystal is concerned. In OGIXOT, large synthons are not affected by the additional hydrogen-bond donor and maintain their linearity as above. They adopt the form of tubes which are composed of O—H···O hydrogen-bonded zigzag chains running along the [010] direction. Additional N—H···O hydrogen bonds link molecules along these chains. Tubes are aligned in parallel. Thus, C—H···π interactions are more directional than those in (**1**). Finally, they join all tubes into a 3D network characterized by a rectangular brickwall cross-section when viewed along [010] (Fig. 5*a*). The interaction energies between neighbouring molecules either in (**1**) or OGIXOT were calculated using the CE-HF/3-21G and CE-B3LYP/6-31G(d,p) benchmarked energy models by the *Crystal Explorer* module (Version 17.5; Turner *et al.*, 2017). Table 5 summarizes the representative energy decomposition into electrostatic, polarization, dispersion and repulsion components. The energy frameworks (Fig. 5*b*) are in a good agreement with the large synthon concept.

In (**1**), the electrostatic component is a driving force for the strongest interactions (total energy ∼55 kJ mol^{-1}) between molecules joined by O—H···O hydrogen bonds and forming the large chain synthon. The secondary weak interactions are mostly attractive due to the substantial dispersion energy term and the total energy approaching 40 kJ mol^{-1} for C—H···π contacts between Fmoc fragments and ∼30 kJ mol^{-1} for weak interactions, which propagate along the [001] direction. Therefore, these secondary weak contacts are important for crystal formation. Their relatively high energy compared to the value calculated for the basic motif may result from their co-operativity. The latter corresponds to the number of hydrogen-bonded motifs found in (**1**). For OGIXOT, the strongest interactions are the peptide N—H···O hydrogen bonds. Their energy was estimated to be around 90 kJ mol^{-1}. In the $C(4)$ chain motif formed by carboxyl groups, the O—H···O contacts are of comparable energy (∼40 kJ mol^{-1}) to C—H···π Fmoc–Fmoc and phenyl–phenyl interactions (Table 5). This might result from repulsion between the O atoms in the motif (E_{rep} = 69.4/53.1 kJ mol^{-1} for DFT/HF) and therefore outweighs the electrostatic contribution (E_{ele} = −47.2/−53.7 kJ mol^{-1} for DFT/HF), consequently weakening these relatively strong interactions. The Fmoc–phenyl interactions in OGIXOT are twice as weak. It is noteworthy that in the remaining Fmoc–Tyr/Phe derivatives (each possesses a hydrogen-bond-active N—H donor group), the peptide N—H···O hydrogen bond leads to the formation of a large 1D synthon, whereas the –COOH groups interact mostly with solvent molecules. Taking into account the energies in the large synthon in OGIXOT and the relatively high energy of the peptide hydrogen bond in comparison to hydrogen bonds with the –COOH group, it seems that the carboxyl group might be more likely to interact with a solvent molecule than the rest of the peptide. Only in Z-shaped molecules characterized by CH(fmoc)—CH_2···C*—CH_2(Ph) (τ) pseudo-torsion angles close to 90°, like OGIXOT, OGIXUZ, XATJEK and XATKIP, may the interactions between 1D large synthons be regarded as directional. For V-shaped molecules, τ is in the range from 10 to 40° [(**1**), INEJEQ, OGOGIA, WATSIU01, XATJAG and XATKEL]. They exhibit close to or even an exact hexagonal packing of rods, like XATJAG and XATKEL, which crystallize in the space group $P6_3$. The rotamers with an L-shape (τ close to 180°; CAMLEK, OGIYAG, UQIYUG and UQOGUE) form either close to hexagonal packing (UQIYUQ and UQOGUE) or a 2D layer motif (OGIYAG and CAMLEK). In the two latter structures, as well as in WATSIU01, additional hydrogen-bond donors linked to the phenyl ring are present. This leads to the formation of large 2D synthons.

The auxiliary ellipsoid plots for Fmoc–Tyr/Phe structures are shown in Fig. S4 in the supporting information. Supramolecular hydrogen-bond patterns formed by the fluorenyl moiety in the structures retrieved from the CSD are presented in Fig. 6. Other hydrogen-bond motifs are illustrated in Fig. S5 in the supporting information.

3.3.3. Quantitative analysis of the supramolecular packing. The Kitaigorodsky Packing Index (KPI) (Kitaigorodskii, 1961, 1973) was calculated with the '*calc void*' routine as implemented in *PLATON* (Spek, 2020). Results revealed that the percentages of filled space are 66.7 and 70.1% in (**1**) and OGIXOT, respectively, and indicate a tight packing of the molecules in the crystal. No space accessible for solvents was found. The remaining Fmoc–Tyr/Phe derivatives are characterized by similar KPI values, from 62.9% in MOXSUP to 71.6% in UQOGUE (see Table 2). Thus, MOXSUP is the most

Table 6
Occurrence of supramolecular synthons in all Fmoc–AAs.

		Fmoc–Tyr/Phe derivatives	Other Fmoc-based AA derivatives
S(6)	(**C**H$_2$)···(C═**O**)	OGIYAG, DULLAZ, MOXSUP	
S(11)	(CH$_{cycl}$)···(C═**O**)	EKEWUM	QOFHID (Ile)
C(4)	(**C**H)···(C═**O**)	(**1**), NUBPEH	
	(**O**H)···(C═**O**)	OGIXOT, CAMLEK, UQIYUQ, UQOGUE, XATJAG, XATJEK, XATKEL	QOFHID (Ile)
	(**N**H)···(C═**O**)	OGIXOT, INEJEQ, OGOGIA, NUBPEH, OGIXUZ, VERXUO, XATJAG, XATJEK, XATKEL, XATKIP	CUWKOU01 (Ala), XAVYIE (Gly), EXOFAY (Orn)
C(5)	(**C**H$_2$)···(C═**O**)	OGIYAG, CAMLEK, DULLAZ, EKEWUM, MOXSUP, UQIYUQ, UQOGUE, XATJAG, XATKEL	VERQOB (Gly), BIZXUE (Leu), DIZNIK (Trp)
	(**C**H)···(C−**O**−C)	OGIYAG, CAMLEK, EKEWUM, UQIYUQ, UQOGUE	QOFHID (Ile), BIZXUE (Leu), MOHCIW (Ser), DIZNIK (Trp)
	(**N**H)···(C═**O**)	CAMLEK	ADAGOE (Ser)
	(**N**H)···(C−**O**−C)	EKEWUM	DIZNIK (Trp)
	(**N**H)···(**O**H)	UQIYUQ, UQOGUE	QOFHID (Ile) BIZXUE (Leu)
C(6)	(**C**H$_2$)···(C−**O**−C)	DULLAZ, MOXSUP	
C(7)	(**O**H)···(C═**O**)	(**1**)	ADAGUK (Ala), VERXIC (Gly), VERXOI (Gly), BIZXUE (Leu), MOHCIW (Ser)
C(8)	(**C**H$_{cycl}$)···(C═**O**)	INEJEQ, EKEWUM	ADAGUK (Ala), VERQER (Gly), VERQIW (Gly), VERXIC (Gly), MOHCIW (Ser)
	(**C**H$_2$)···(C═**O**)		VERQOB (Gly), VERXIC (Gly), VERXOI (Gly), BIZXUE (Leu), MOHCIW (Ser)
C(11)	(**C**H$_2$)···(C═**O**)	OGOGIA	DIZNIK (Trp)
C(12)	(**C**H$_{cycl}$)···(C═**O**)	EKEWUM	ADAGUK (Ala)
	(**C**H$_{cycl}$)···(**O**H)		VERQER (Gly), VERXIC (Gly), VERXOI (Gly)
C(13)	(**C**H$_{cycl}$)···(**O**H)	XATJEK	ADAGUK (Ala)
C(14)	(**C**H$_{cycl}$)···(**F**)		VERQIW (Gly), VERQOB (Gly)
C_2^1(8)	(**C**H$_2$)···(C═**O**)		VERQIW (Gly), VERXIC (Gly)
C_2^2(7)	(**O**H)···(C═**O**) & (**O**H)···(**N**H)	CAMLEK, UQIYUG, UQOGUE	QOFHID (Ile)
C_2^2(8)	(**C**H)···(C–**O**–C) & (**O**H)···(C═**O**)		BIZXUE (Leu), MOHCIW (Ser)
C_2^2(9)	(**O**H)···(C═**O**) & (**O**H)···(**N**H)	CAMLEK, UQIYUQ, UQOGUE	QOFHID (Ile)
	(C═**O**)···(**O**H) & (C═**O**)···(**C**H$_2$)	XATJAG	VERQIW (Gly), VERXIC (Gly), MOHCIW (Ser)
C_2^2(10)	(**N**H)···(C═**O**) & (**C**H)···(C−**O**−C)	EKEWUM	BIZXUE (Leu)
	(**N**H)···(**O**H) & (**C**H)···(C−**O**−C)	UQIYUQ, UQOGUE	QOFHID (Ile)
	(**C**H$_2$)···(C═**O**) & (**C**H)···(C-**O**-C)	EKEWUM, UQIYUQ, UQOGUE	BIZXUE (Leu), DIZNIK (Trp)
C_2^2(10)	(**C**H$_{cycl}$)···(C═**O**) & (**C**H$_{cycl}$)···(**O**H)		ADAGUK (Ala), VERQER (Gly), VERXIC (Gly)
	(**C**H$_{cycl}$)···(**O**H) & (**C**H$_2$)···(C═**O**)		VERQIW (Gly), VERQIW (Gly), VERXOI (Gly)
	(**C**H$_3$)···(C−**O**−C) & (**C**H$_{cycl}$)···(C═**O**)	INEJEQ, EKEWUM	
	(**C**H$_2$)···(C═**O**) & (**C**H)···(C−**O**−C)	CAMLEK, OGIYAG, DULLAZ	
C_2^2(11)	(**O**H)···(C═**O**) & (**C**H)···(C═**O**)	(**1**)	VERQIW (Gly)
	(**C**H$_2$)···(C═**O**) & (**C**H$_2$)···(C−**O**−C)	DULLAZ, MOXSUP	
	(**C**H)···(C−**O**−C) & (**O**H)···(C═**O**)	UQIYUQ, UQOGUE	QOFHID (Ile)
	(**C**H$_{Fmoc}$)···(**N**O$_2$) & (**C**H$_2$)···(**N**O$_2$)	UQOGUE	
	(**N**H)···(C═**O**) & (**C**H$_2$)···(C═**O**)	XATJAG, XATKEL	
C_2^2(11)	(**O**H)···(C═**O**) & (**C**H$_{cycl}$)···(**O**H)		VERQIW (Gly), VERXIC (Gly), VERXOI (Gly)
	(**O**H)···(C═**O**) & (**C**H$_2$)···(C═**O**)		VERQIW (Gly), VERXIC (Gly)
C_2^2(12)	(**O**H)···(C═**O**) & (**N**H)···(C═**O**)	OGIXOT, XATJAG, XATJEK, XATKEL,	BIZXUE (Leu)
	(**N**H)···(**O**H) & (**C**H$_2$)···(C═**O**)	CAMLEK, UQIYUQ, UQOGUE	
	[(**C**H$_2$)···(C═**O**)]$_2$	CAMLEK	VERXIC (Gly)
	(**N**H)···(C═**O**) & (**C**H$_{cycl}$)···(C═**O**)	INEJEQ, EKEWUM	
	(**C**H$_{cycl}$)···(C═**O**) & (**C**H$_2$)···(C═**O**)		VERXIC (Gly), MOHCIW (Ser)
	(**O**H)···(C═**O**) & (**C**H)···(C−**O**−C)		BIZXUE (Leu), MOHCIW (Ser)
C_2^2(13)	[(**C**H$_2$)···(C═**O**)]$_2$		VERQOB (Gly), BIZXUE (Leu)
	(**C**H$_2$)···(C═**O**) & (**C**H)···(C−**O**−C)		BIZXUE (Leu), MOHCIW (Ser)
C_2^2(14)	[(**C**H$_2$)···(C═**O**)]$_2$	DULLAZ, MOXSUP	
	(**C**H$_{cycl}$)···(**O**H) & (**C**H$_2$)···(C═**O**)		VERQIW (Gly), VERXIC (Gly)
C_2^2(15)	(**O**H)···(C═**O**) & (**C**H$_2$)···(C═**O**)	CAMLEK, UQOGUE	VERQIW (Gly), VERXIC (Gly), VERXOI (Gly), BIZXUE (Leu)
	(**O**H)···(C═**O**) & (**C**H$_{Fmoc}$)···(**O**H)	OGIXUZ, XATJEK	
	(**O**H)···(C═**O**) & (**C**H$_{cycl}$)···(C═**O**)		ADAGUK (Ala), VERXIC (Gly)
	(**N**H)···(C═**O**) & (**C**H$_{Fmoc}$)···(**Cl**$_1$)	XATJEK	
	(**N**H)···(C═**O**) & (**C**H$_{Fmoc}$)···(**O**H)	XATJEK	
	(**C**H)···(**Cl**) & (**O**H)···(**C**H$_{Fmoc}$)	XATJEK	
	(**C**H$_{cycl}$)···(**O**H) & (**C**H$_2$)···(C═**O**)		VERQIW (Gly), VERXIC (Gly)
	(**C**H$_{cycl}$)···(C═**O**) & (**C**H$_2$)···(C═**O**)		VERXIC (Gly), VERXOI (Gly), MOHCIW (Ser)
C_2^2(19)	(**O**H)···(C═**O**) & (**C**H$_2$)···(C═**O**)	OGIYAG, UQOGUE	
	(**C**H$_{cycl}$)···(C═**O**) & (**O**H)···(C═**O**)	DULLAZ	ADAGUK (Ala), QOFHID (Ile)
C_2^2(19)	(**O**H)···(C═**O**) & (**C**H$_{cycl}$)···(**O**H)		VERQIW (Gly), VERXIC (Gly), VERXOI (Gly)
	(**C**H$_{Fmoc}$)···(**N**O$_2$) & (**C**H$_2$)···(C═**O**)	UQOGUE	
C_2^2(20)	(**C**H$_{cycl}$)···(C═**O**) & (**C**H$_{cycl}$)···(**O**H)		VERQER (Gly), VERXIC (Gly)

Table 6 (continued)

		Fmoc–Tyr/Phe derivatives	Other Fmoc-based AA derivatives
	(**C**H$_2$)···(C═**O**) & (**C**H$_{cycl}$)···(**O**H)		VERQIW (Gly), VERXIC (Gly), VERXOI (Gly)
$C_4^4(20)$	(**O**H)···(C═**O**) & (**C**H)···(C—**O**—C)		BIXUE (Leu), MOHCIW (Ser)
	(**C**H)···(C—**O**—C) & (**C**H$_2$)···(C═**O**)		BIXUE (Leu), MOHCIW (Ser)
$R_2^2(8)$	(**N**H)···(**O**H) & (**C**H)···(C—**O**—C)	CAMLEK, UQOGUE	QOFHID (Ile)
	(**C**H$_2$)···(C═**O**) & (**C**H)···(C—**O**—C)	CAMLEK, OGIYAG, EKEWUM, UQIYUQ, UQOGUE	BIZXUE (Leu), DIZNIK (Trp)
	[(**O**H)···(C═**O**)]$_2$	DULLAZ, MOXSUP	VERQER (Gly), VERQOB (Gly)
	(**N**H)···(C—**O**—C) & (**C**H)···(C—**O**—C)	EKEWUM	DIZNIK (Trp)
$R_2^2(9)$	(**C**H$_2$)···(C—**O**—C) & (**C**H$_2$)···(C═**O**)	OGOGIA, MOXSUP	
	[(**C**H$_2$)···(C═**O**)]$_2$	DULLAZ	VERQOB (Gly)
$R_2^2(9)$	(**O**H)···(C═**O**) & (**C**H$_2$)···(C═**O**)		VERQIW (Gly), VERXIC (Gly), VERXOI (Gly), BIZXUE (Leu)
$R_2^2(12)$	(**C**H$_2$)···(C═**O**) & (**N**H)···(C—**O**—C)	EKEWUM	DIZNIK (Trp)
$R_2^2(14)$	(**C**H$_3$)···(C═**O**) & (**N**H)···(C═**O**)	INEJEQ, NUBPEH	
	[(**C**H$_2$)···(C═**O**)]$_2$	DULLAZ, MOXSUP	XAVYIE (Gly)
$R_3^3(11)$	(**N**H)···(**O**H) & (**O**H)···(C═**O**)	CAMLEK, UQIYUQ, UQOGUE	QOFHID (Ile)
$R_3^3(15)$	(**O**H)···(C═**O**) & (**C**H)···(C—**O**—C)	CAMLEK, UQIYUQ, UQOGUE	QOFHID (Ile)
$R_3^3(19)$	(**O**H)···(C═**O**) & (**C**H$_2$)···(C═**O**)	CAMLEK, UQIYUQ, UQOGUE	
$R_4^4(16)$	(**O**H)···(C═**O**) & (**N**H)···(**O**H)	UQIYUQ, UQOGUE	QOFHID (Ile)
$R_4^4(20)$	(**O**H)···(C═**O**) & (**C**H)···(C—**O**—C)		BIZXUE (Leu), MOHCIW (Ser)
	(**C**H$_2$)···(C═**O**) & (**C**H)···(C—**O**—C)		BIZXUE (Leu), MOHCIW (Ser)

closely packed structure among the investigated Fmoc–Tyr/Phe AAs.

3.4. A library of supramolecular hydrogen-bonding patterns

3.4.1. Substituent effect on the supramolecular assembly of Fmoc–Tyr/Phe AAs. In comparison with other so far known Fmoc–Tyr/Phe crystal structures, we managed to build a gallery of supramolecular hydrogen-bonding synthon patterns (Table S7 in the supporting information). The occurrence of supramolecular synthons is summarized in Table 6. *D*—H···*A* (*D* is donor and *A* is acceptor) angles greater than 120° (and motifs engaging less than 20 atoms) were taken into account. We observed a significant effect of the influence of various

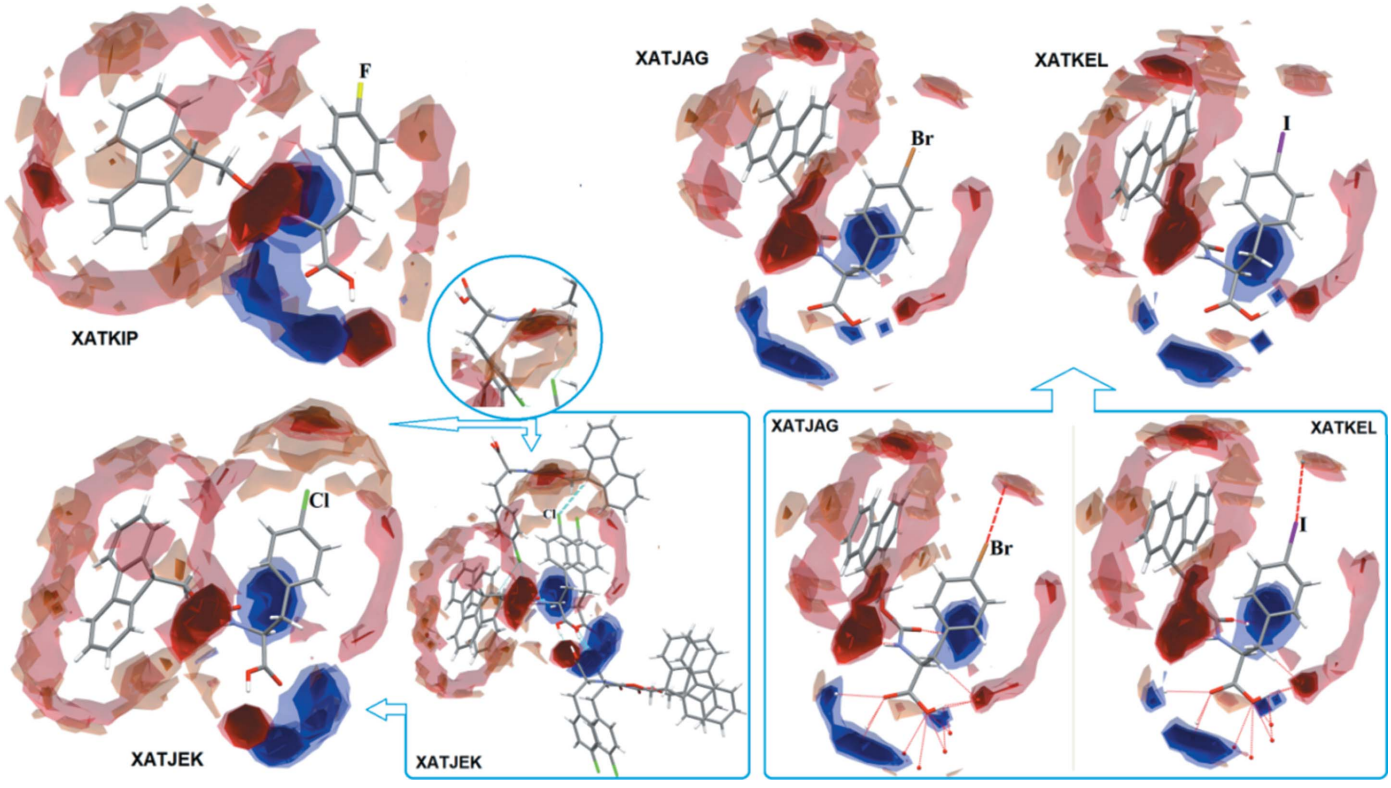

Figure 7
Full interaction maps (FIMs) for XATKIP, XATJEK, XATJAG and XATKEL (Pizzi *et al.*, 2017), showing the preferences of the interactions (blue regions indicate the presence of hydrogen-bond donors and red areas indicate the presence of hydrogen-bond acceptors).

types of substituents in the core of the structure on the creation of supramolecular synthons and patterns. Among the Fmoc–Tyr/Phe AAs, homosynthons $C_2^2(12)$, $C_2^2(14)$, $R_2^2(9)$, $R_2^2(14)$, between –$\mathbf{C}H_2$ and –C═**O** functional groups, and $R_2^2(8)$ between –**O**H···C═**O** functionalities are observed. Additionally, it is worthy of mention that the presence of halogens affects the supramolecular patterns in the Fmoc–AA family. In particular, in XATKEL (Pizzi *et al.*, 2017), C—I···π interactions between an I atom and fluorenyl [I···(centroid of phenyl ring) distance is 3.829 Å and C—I···(centroid of phenyl ring) angle is 165.27°] give rise to the formation of supramolecular rings. In XATJAG (Pizzi *et al.*, 2017), those rings are created by C—Br···π interactions. Thus, supramolecular halogenated motifs are interchangeable with molecular halogenated synthons. Supramolecular patterns created by weak (Fmoc)C—H···O, (Fmoc)C—H···Cl, C—Br···π(Fmoc) and C—I···π(Fmoc) interactions are illustrated in Fig. 6. The *Full Interaction Maps* (FIMs) tool (Wood *et al.*, 2013) was used to generate a picture of the interaction landscape of molecules [from three-dimensional (3D) coordinates]. In this way, the most likely locations for a variety of functional groups were predicted. As a consequence, C—H···O hydrogen-bonding motifs in the class of Fmoc–AAs were estimated. Generally, the fluorene system is able to take part in C—H···O interactions, in agreement with the FIMs. We also investigated the differences in the interaction preferences of a molecule in the context of subtle changes in the substitutions of the phenyl ring, replacing fluorine (XATKIP) with chlorine (XATJEK), bromine (XATJAG) and iodine (XATKEL) (Pizzi *et al.*, 2017). We compared the generated maps. As can be seen from Fig. 7, with the growing size of the halogen, the probability of finding an acceptor interacting with the halogen increases. This interaction is absent for the fluoro and chloro derivatives, but visible for the bromo and iodo analogues. Moreover, the intramolecular graph-set motifs, namely $S(6)$, created by (CH_2)C—H···O(═C), occur in OGIYAG, DULLAZ and MOXSIP, while $S(11)$ formed through (CH_{cycl})C—H···O(═C) occurs in EKEWUM. The title crystal, (**1**), participates in the following supramolecular motifs: $C(4)$ *via* C—H···O(═C), $C(7)$ by O—H···O(═C) and $C_2^2(11)$ through O—H···O(═C) and C—H···O(═C) interactions. On the other hand, OGIXOT is involved in a $C_2^2(12)$ pattern by O—H···O(═C) and N—H···O(═C) interactions. $C(14)$, $C_2^2(8)$, $C_2^2(13)$, $C_2^2(20)$ and $R_4^4(20)$ motifs are not observed in Fmoc–Tyr/Phe derivatives, while $S(6)$, $C(4)$, $C(6)$, $R_2^2(9)$ and $R_3^3(19)$ motifs are created only in the crystals of Fmoc–Tyr/Phe derivatives. The Fmoc group participates in the formation of a supramolecular $C_2^2(15)$ chain *via* (Fmoc)C—H···OH and O—H···O(═C) interactions in OGIXUZ and XATJEK. Nevertheless, hydrogen-bonding patterns formed by the Fmoc moiety are observed much more frequently. Interestingly, in the context of all Fmoc–Tyr/Phe derivatives, the shortest π–π interactions are observed in EKEWUM [*Cg*(fluorene)···*Cg*(fluorene)-(x − 1, y, z) = 3.729 (4) Å], while the shortest C—H···π interactions are observed in WATSIU01 (H···*Cg* = 2.63 Å).

3.4.2. A case study of other types of Fmoc–AA. Furthermore, we extended our work to consider other types of Fmoc–AAs found in the CSD. Among them, similar supramolecular features are observed (Table 6, and Table S7 in the supporting information). The most frequently observed arrangements of molecules are chains engaged in C—H···O contacts. In particular, there are $C(8)$ synthons, between –CH_{cycl} and

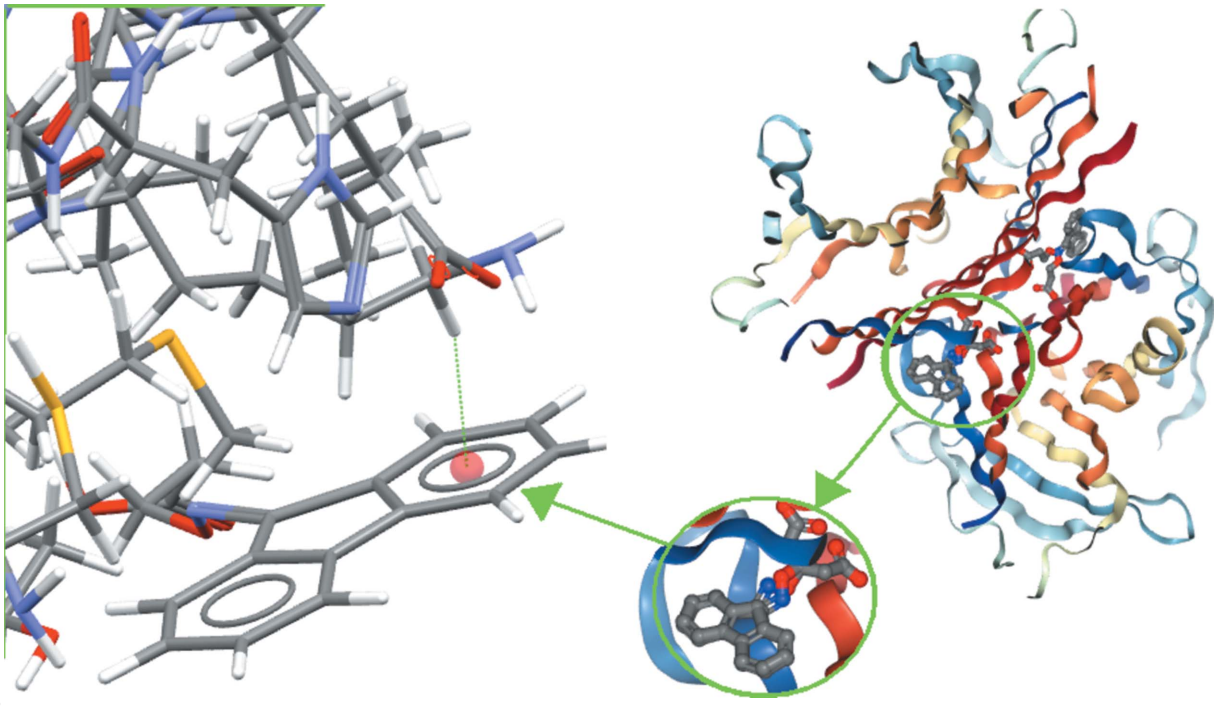

Figure 8
Partial packing of a biocomplex showing the C—H···π(Fmoc) interaction (PDB code 3gs4; Palaninathan *et al.*, 2009).

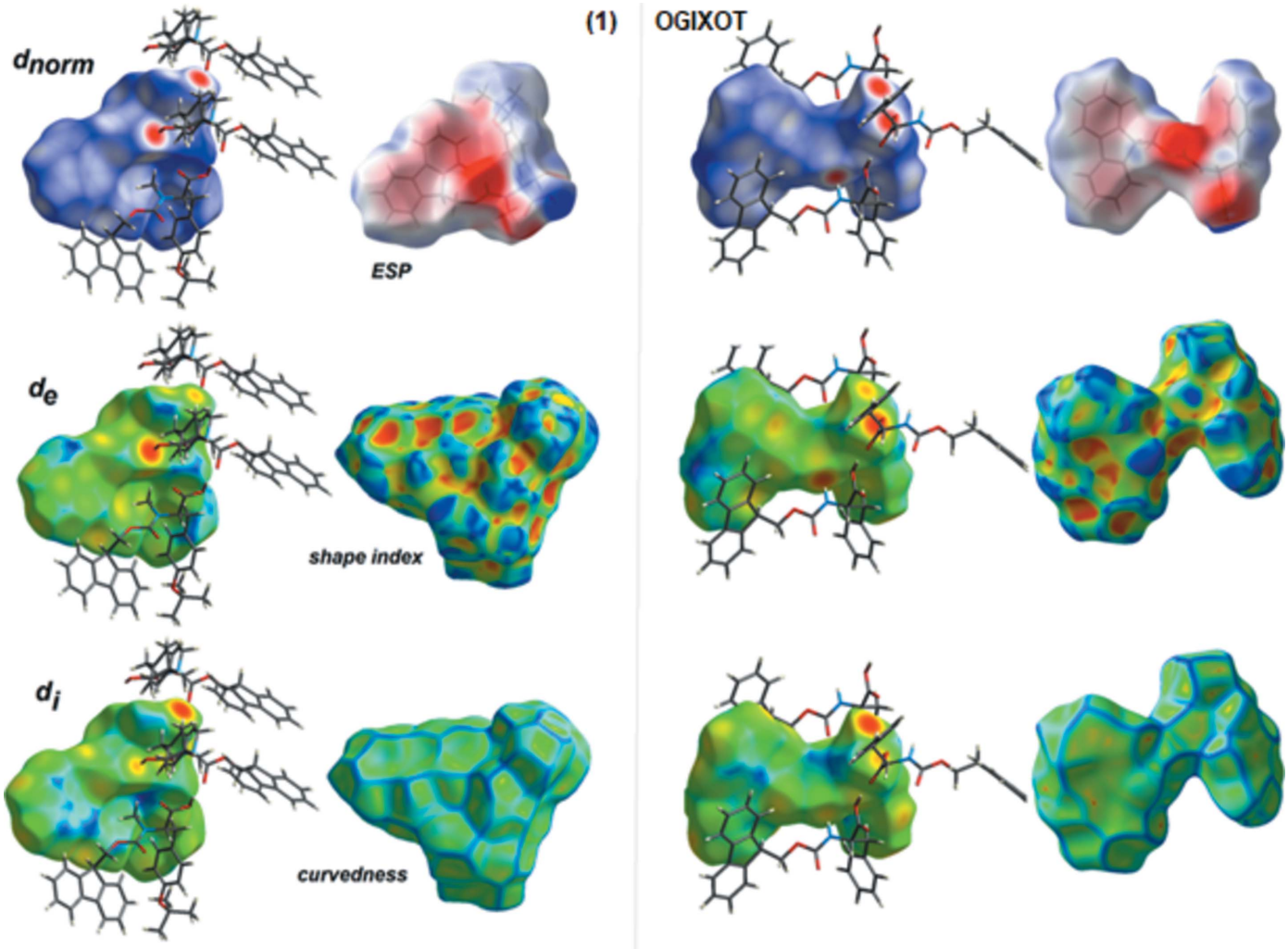

Figure 9
Hirshfeld surfaces mapped with d_{norm}, shape index and curvedness, and ESPs for the main structures in (**1**) and OGIXOT (Draper *et al.*, 2015).

O═C– or –CH_2 and O═C functionalities, and also $C(7)$ synthons, between –OH and O═C functional groups, in mainly Fmoc–Ala and Fmoc–Gly derivatives (but also in Fmoc–Leu or Fmoc–Ser). The latter is observed in (**1**) also. Another synthon common for (**1**) and Fmoc–Gly is $C_2^2(11)$ between **O**—H···**O**(═C) and **C**—H···**O**(═C), while for OGIXOT and Fmoc–Leu a common synthon is $C_2^2(12)$ between **O**—H···**O**(═C) and **N**—H···**O**(═C). In addition, unique synthons for other types of Fmoc–AAs, not observed in the Fmoc–Tyr/Phe crystals, such as $C_2^2(8)$, $C_2^2(11)$, $C_2^2(13)$, $C_2^2(19)$, $C_2^2(20)$, $C_4^4(20)$ and $R_4^4(20)$, were found as well. To sum up, although the structural modification in the Fmoc–AA backbone (*i.e.* introduction of other functional groups) is related to the conformational changes and diversity of hydrogen-bonding supramolecular patterns, characteristic correlations can be noticed.

3.5. A first look at Fmoc-based interactions in biocomplexes

Fmoc–AAs can be bioligands of diverse proteins. Targeting protein–peptide interactions is an attractive approach for state-of-the-art drug discovery and design (Ciemny *et al.*, 2018). Efficient geometry and binding-mode descriptors are crucial for understanding protein–ligand interactions. Comprehensive synthon libraries may be useful when applied to searches for binding sites of diverse bioligands fostering new active-site discoveries. This view is supported by the recent report of Bulusu & Desiraju (2019) who pointed out that the combination of the knowledge base gained from better quality protein–ligand structures with theoretical models will be a challenge in the near future. Our results indicate that weak C—H···π interactions are crucial for the stability of the Fmoc–AA supramolecular architectures and prompted us to examine the Fmoc–AA binding mode in a structure of transthyretin cocrystallized with a fluorene-containing derivative of propionic acid. The former is a protein controlling amyloid fibril formation, while the latter is an active neuroprotector used in the treatment of Alzheimer's disease (Silva *et al.*, 2017; Palaninathan *et al.*, 2009). The C—H···π(Fmoc) interaction, which controls the cofactor binding, is presented in Fig. 8. A similar situation is observed for 40 relevant macromolecular species reported in the PDB (Bojarska *et al.*, 2019*c*,*d*). Further advanced *in silico* studies are in progress and will be reported in the future.

3.6. Hirshfeld surface (HS) studies

3.6.1. HS maps and molecular electrostatic potentials: (1) *versus* other Fmoc–Tyr/Phe crystals. HS analysis (Spackman & Jayatilaka, 2009) was employed to identify, visualize and gain a deeper knowledge of the weak interactions in crystals of Fmoc–AAs. Generally, this confirmed the occurrence of all interactions in (**1**) identified by *PLATON* (Spek, 2020) and described in the previous subsection. The directions and strengths of the interactions were mapped onto the HS maps using the d_{norm}, d_e and d_i descriptors. The intense red spots on the d_{norm} maps signify electron-rich regions that actively participate in strong intermolecular O—H···O hydrogen bonding between carboxyl H and carbonyl O atoms (Venkatesan *et al.*, 2016). Precisely, the d_i profile indicates O—H···O and d_e indicates O—H···O hydrogen bonds. On the other hand, the light-red spots characterize N—H···O hydrogen bonds in the case of (**1**) and weak C—H···O interactions in both (**1**) and OGIXOT. The white areas are related to subtle H···H contacts. Closer examination revealed essential differences in the subtle interactions across (**1**) and OGIXOT (Draper *et al.*, 2015). The latter presents the minor contribution of π–π stacking interactions signified by the conterminous small red and blue triangles and flat curvature green regions *via* blue outlines on the shape index and curvedness maps, respectively (Fig. 9). The molecular electrostatic potentials (ESP), mapped over the HSs of (**1**) and OGIXOT, provide a further insight into the character of the interactions, showing the positions of the close contacts. At first glance, they reveal similarly distributed positive (blue areas) and negative (red) parts. The ESP in (**1**) indicates interactions between complementary electronegative regions (hydrogen-bond acceptors) of the *N*-fluorenylmethoxycarbonyl-*O*-*tert*-butyl-*N*-methyltyrosine molecule with electropositive areas (hydrogen-bond donors) of neighbouring molecules in the crystal packing. Most of the charge regions correspond to contacts visible on the d_{norm}-mapped HS, presenting the donor and acceptor natures of the atoms. A thorough inspection shows some dissimilarity, with one area being more electronegative than the other. This means different kinds of interactions. For example, atom O2 does not participate in strong interactions. The ESP for all Fmoc–Tyr/Phe crystals are presented in Fig. S6 in the supporting information.

3.6.2. Intermolecular interaction survey: quantitative analysis.

Fingerprint plots (FPs) in Fmoc–Tyr/Phe derivatives. Full FPs for (**1**) and OGIXOT show a dissimilarity in relation to the C···H/H···C interactions. The plots exhibit two pairs of sharp spikes in (**1**) *versus* one pair in OGIXOT, corresponding to C···H/H···C and O···O/H···O contacts, and one obtuse angle between these pairs of spikes, corresponding to H···H interactions. The latter are reflected in the scattered points in the large surface of the FP plots. Decomposed FP plots show minor but significant differences between both compounds (Fig. S7 in the supporting information). In (**1**), the H···H contacts represent the largest relative contribution, amounting to 61%. The C···H/H···C contacts share 22%, while the

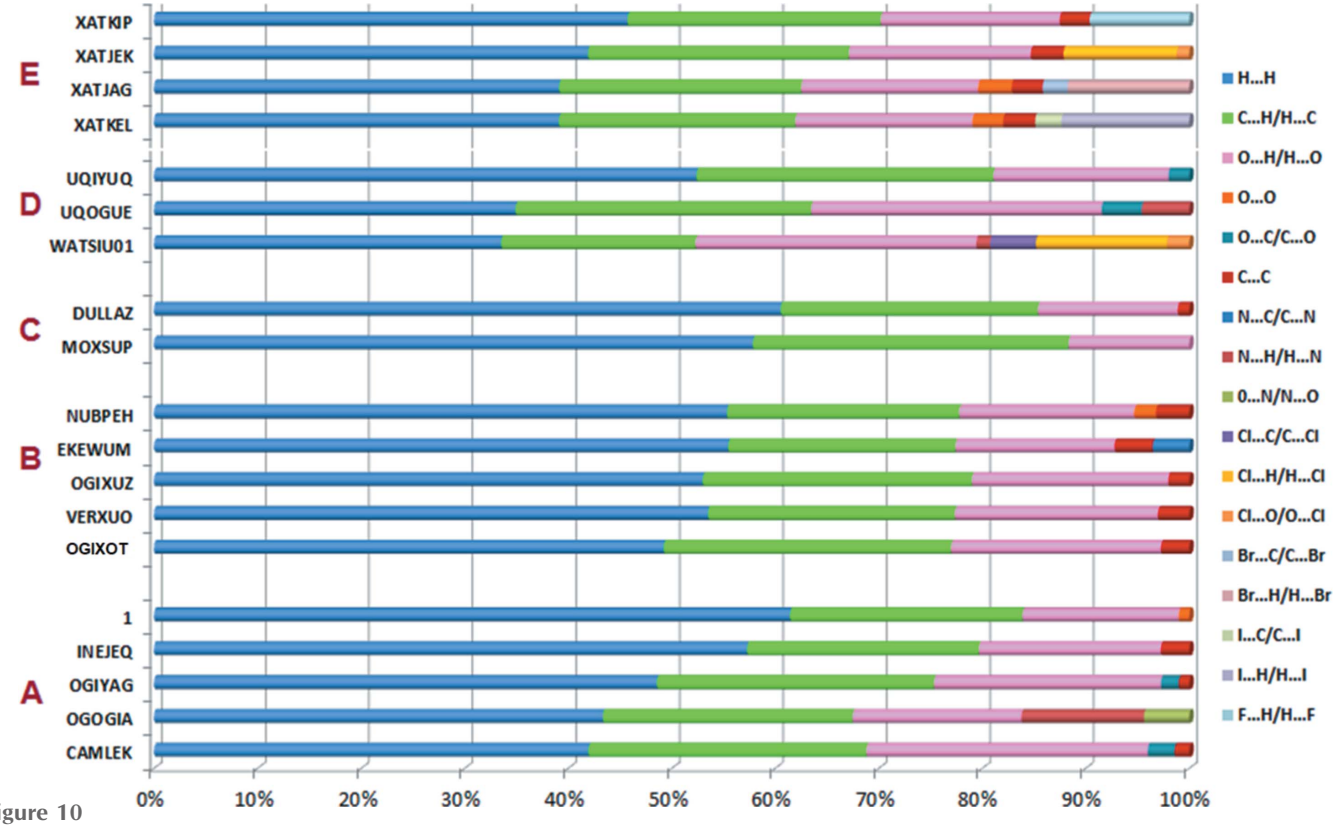

Figure 10
The percentage contributions to the Hirshfeld surface area for all intermolecular contacts involved in the structure of (**1**) and related Fmoc–Tyr/Phe derivatives retrieved from the CSD.

O···H/H···O interactions share 15%. Thus, C—H···O are the major noncovalent interactions in the title compound. The large contribution of the C···H/H···C contacts is a result of the presence of unsaturated C atoms and H···π interactions. O···O (lone pair–lone pair) and O···C/C···O (lone pair–π/π–lone pair) interactions are observed at the level of 1%. On the other hand, in OGIXOT, higher shares of O···H/H···O and C···H/H···C interactions are observed. Moreover, C···C (π–π) contacts, instead of O···C/C···O and O···O, are observed. Furthermore, we focused our attention on structural modifications in the molecular structure core of Fmoc–AAs on the interactions. The relative percentage contributions to the HS area for the majority of particular interactions in the packing arrangements in crystals are summarized in Fig. 10, and Table S8 in the supporting information. Decomposed FP histograms are shown in Fig. S8 in the supporting information. Fmoc–Tyr(Phe) derivatives have structural similarities. Overall, the main interactions, such as H···H, C···H/H···C and O···O/H···O, present the largest share, from 77% in WATSIU to 99% in MOXSUP. However, H···H interactions are the greatest contributor, comprising about half of the total HS area [from 33% in WATSIU to 61% in (**1**)], which is obvious due to a higher proportion of H atoms. These subtle interactions act as *sticky fingers* gluing supermolecules together. Interestingly, strong O···H/H···O hydrogen bonds contribute only 20% of the total interactions, arising from the lowest participation in MOXSUP (12%) to the highest in UQOGUE (27%). The appreciable increasing portion of these hydrogen bonds is interpreted by the presence of multiple –OH, –C═O, –O–, –COOH and –NO_2 functionalities. The O···H/H···O interactions have lower values than C···H/H···C. A deeper insight revealed additional features. In group **A**, N···O/O···N interactions are observed (~4% in OGOGIA) due to the presence of NO_2. In groups **B** and **E**, π–π stacking contacts provide contributions worthy of discussion. Their occurrence, among structures with a contribution above 3%, follows the order: VERXUO and XATKEL (3%), XATJEK (3.1%), NUBPEH (3.2%) and EKEWUM (3.6%). Notably, significant C···C contacts are not only observed in the (**1**) and MOXSUP structures. In group **C**, only H···H, O···H/H···O and C···H/H···C interactions are present. In groups **D** and **E**, the highest diversity of interaction types is observed. In particular, the substitution in the phenyl ring by halogen atoms (XATJEK, XATKIP, XATJAG and XATKEL) leads to the appearance of halogen interactions, such as Br···C(H), F···H, I···C(H) and Cl···H(C,O). Interestingly, the latter are also observed in group **D**, in WATSIU01. In groups **A** and **D**, C···O/O···C contacts are noticeable (with the highest value of 3.8% in UQOGUE) due to the O-atom substituent in the phenyl ring. In group **D**, the supramolecular assemblies are additionally stabilized by N···H/H···N interactions because of substitution of the N atom in the phenyl ring (the highest contribution is 4.5% in UQOGUE); these are important to rationalize the solid-state crystal structures. Surprisingly, modification of the –COOH group has no further relevance to the percentage contributions of interactions. Nevertheless, additional supramolecular synthon patterns, in which a modified –COOH group is engaged, are visible [in OGOGIA: $C(15)$, $C_2^2(10)$ and $C_2^2(13)$; in INEJEQ: $C(6)$, $C(12)$, $C_2^2(16)$, $C_2^2(20)$, $R_2^2(14)$ and $R_2^2(16)$].

In addition, some physiochemical properties and quantitative measures of HSs (calculated with *CrystalExplorer* and *PLATON*), such as Hirshfeld molecular volume (V), surface area (A), globularity (G), which is 'a measure of the degree to which the surface area differs from the value for a sphere of the same volume' (Meyer, 1986), and asphericity (Ω), which is 'a measure of the anisotropy of an object when applied to the atomic positions' (Rudnick & Gaspari, 1986; Baumgärtner, 1993) are summarized in Table S9 of the supporting information. The intermediate target was determination of the molecular surface nature and the anisotropy of the studied molecules. G values below 1 indicate that the molecular surface is more structured (not spherical).

Other types of Fmoc–AAs. The percentage contributions to the HS area for the corresponding interactions in the crystal packing of other types of Fmoc–AAs are shown in Fig. S9 and Table S10 in the supporting information. As we can see, in the family of Fmoc–Gly derivatives, H···H contacts have the lowest participation. In the crystals of VERQER and VERQOB, F···H/H···F interactions have the major contributions, at a level of ~25%, while F···F and F···C/C···F are important as well. This is caused by introduction of the F atom into the structure. In VERXIC, C···O/O···C (4%) and N···H/H···N (1.5%) interactions are remarkable. C···C contacts have the highest contribution in Fmoc–Ala/Ser/Ile derivatives (above 2%). Full FPs for all the Fmoc–Tyr/Phe structures are shown in Fig. 11.

3.7. The π–π packing motifs in Fmoc–AAs

With regard of the existence of π–π interactions, we can undertake a more systematic study of the crystal packing and establish some trends. According to the classification of Desiraju & Gavezzotti (1989) and the method of Loots & Barbour (2012), the crystal packing can occur in four structural motifs, in relation to the ratio between the C—H and C—C interactions, calculated by FP analysis, as follows: herringbone (ratio greater than 4.5), sandwich (in the range 3.2–4.0), γ (1.2–2.7; the single outlier at 7.9 is due to a non-aromatic molecule) or β structures (in the range 0.46–1.0). Thereby, in Fmoc–AA crystals, the herringbone motif can be assumed. This motif is constructed from edge-to-face interactions where molecules stack in pairs (Table S11 in the supporting information).

4. Conclusions

In summary, a novel Fmoc–AA, namely *N*-fluorenylmethyloxycarbonyl-*O*-*tert*-butyl-*N*-methyltyrosine, (**1**), was successfully synthesized. It crystallizes in the orthorhombic noncentrosymmetric Sohnke space group $P2_12_12_1$, with one molecule in the asymmetric unit. It forms an interesting supramolecular framework, dominated by classical strong O—

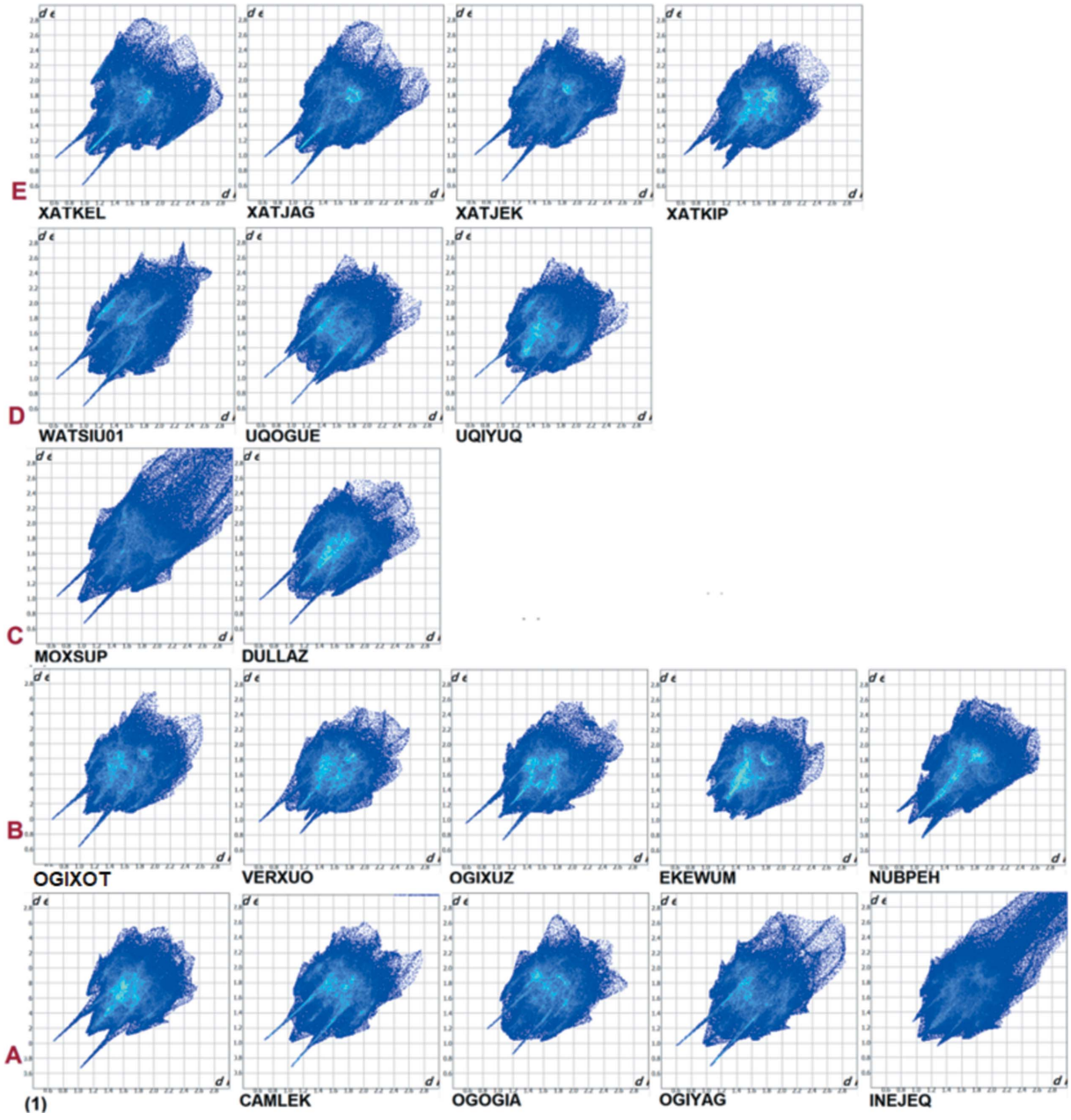

Figure 11
Full FPs for Fmoc–Tyr/Phe derivatives.

H···O and weak C—H···O hydrogen bonds. The Fmoc moiety acts as either a donor or an acceptor in the formation of the supramolecular patterns. The crystal structure of (**1**) was studied in detail and compared with the simplest, most closely related form. Furthermore, a systematic supramolecular study in relation to the family of all known Fmoc–AA derivatives, which can assemble many supramolecular synthon patterns and conformations, has been provided. Due to the variability of the hydrogen-bond patterns, identified interactions are summarized in a short library which may be useful for further studies on the the design/development of smart biofunctional agents. Generally, weak C—H···O, π–π and C—H···π interactions, in which the Fmoc moiety is involved, are significant in this class of compounds. Interestingly, they are also found in related biocomplexes. The most frequently observed arrangements of molecules in the family of Fmoc–AAs are chains engaged in C—H···O contacts. Another insight obtained from this study was the influence of the large rigid planar Fmoc moiety as a supramolecular tecton on the topology of supramolecular assemblies. We hope that our results will provide a compiled knowledge base and a deeper insight into the supramolecular systems of Fmoc–AAs. They may be valuable for scientists interested in the further exploration of unknown Fmoc-based AAs.

References

Adams, D. J. (2011). *Macromol. Biosci.* **11**, 160–173.

Allen, F. H., Kennard, O., Watson, D. G., Brammer, L., Orpen, A. G. & Taylor, R. (1987). *J. Chem. Soc. Perkin Trans. 2*, pp. S1–19.

Al-Mahamad, L. L. G., Horrocks, B. R., Houlton, A. & Waddell, P. G. (2017). Private Communication (refcode CUWKIO01). CCDC, Cambridge, England.

Barone, V. & Cossi, M. (1998). *J. Phys. Chem. A*, **102**, 1995–2001.

Baumgärtner, A. (1993). *J. Chem. Phys.* **98**, 7496–7501.

Becke, A. D. (1988). *Phys. Rev. A*, **38**, 3098–3100.

Becke, A. D. (1993). *J. Chem. Phys.* **98**, 5648–5652.

Berman, H. M., Westbrook, J., Feng, Z., Gilliland, G., Bhat, T. N., Weissig, H., Shindyalov, I. N. & Bourne, P. E. (2000). *Nucleic Acids Res.* **28**, 235–242.

Bernstein, J., Davis, R. E., Shimoni, L. & Chang, N. L. (1995). *Angew. Chem. Int. Ed. Engl.* **34**, 1555–1573.

Bickelhaupt, F. M. & Baerends, E. J. (2000). *Reviews in Computational Chemistry*, Vol. 15, edited by K. B. Lipkowitz & D. B. Boyd, pp. 1–86. New York: Wiley-VCH.

Blaser, G., Sanderson, J. M., Batsanov, A. S. & Howard, J. A. K. (2008). *Tetrahedron Lett.* **49**, 2795–2798.

Bojarska, J., Kaczmarek, K., Zabrocki, J. & Wolf, W. (2018). *Supramolecular Chemistry of Modified Amino Acids and Short Peptides*, in *Advances in Organic Synthesis*, Vol. 11, ch. 2. Sharjah, United Arab Emirates: Bentham Science.

Bojarska, J., Kaczmarek, K., Zabrocki, J. & Wolf, W. (2019*a*). *Int. J. Nutrit. Sci.* **4**, 1–3.

Bojarska, J., Kaczmarek, K., Zabrocki, J. & Wolf, W. (2019*b*). *Nov. Appro. Drug. Des. Dev.* **5**, doi: 10.19080/NAPDD.2019.05.555656.

Bojarska, J., Remko, M., Kaczmarek, K., Zabrocki, J., Zimecki, M. & Wolf, W. M. (2019*c*). *New biologically important synthons in supramolecular chemistry of short peptides*, ECM32, August 2019, Vienna, Austria.

Bojarska, J., Remko, M., Madura, I. D., Wojciechowski, J., Olczak, A., Kaczmarek, K., Zabrocki, J. & Wolf, W. M. (2019*d*). *J. Mol. Struct.* **1190**, 11–22.

Bulusu, G. & Desiraju, G. R. (2019). *J. Indian Inst. Sci.* pp. 1–11.

Ciemny, M., Kurcinski, M., Kamel, K., Kolinski, A., Alam, N., Schueler-Furman, O. & Kmiecik, S. (2018). *Drug Discov. Today*, **23**, 1530–1537.

Clegg, W. & Elsegood, M. R. J. (2003). *Acta Cryst.* E**59**, o1946–o1948.

Cossi, M., Rega, N., Scalmani, G. & Barone, V. (2003). *J. Comput. Chem.* **24**, 669–681.

Desiraju, G. R. (1989). In *Crystal Engineering: The Design of Organic Solids*. Amsterdam: Elsevier.

Desiraju, G. R. (1995). *Angew. Chem. Int. Ed. Engl.* **34**, 2311–2327.

Desiraju, G. R. & Gavezzotti, A. (1989). *Acta Cryst.* B**45**, 473–482.

Diaferia, C., Morelli, G. & Accardo, A. (2019). *J. Mater. Chem. B*, **7**, 5142–5155.

Draper, E. R., Morris, K. L., Little, M. A., Raeburn, J., Colquhoun, C., Cross, E. R., McDonald, T. O., Serpell, L. C. & Adams, D. J. (2015). *CrystEngComm*, **17**, 8047–8057.

Du, X., Zhou, J., Shi, J. & Xu, B. (2015). *Chem. Rev.* **115**, 13165–13307.

Etter, M. C. (1990). *Acc. Chem. Res.* **23**, 120–126.

Etter, M. C. (1991). *J. Phys. Chem.* **95**, 4601–4610.

Farhadi, T. & Hashemian, S. M. R. (2018). *Drug. Des. Dev. Ther.* **12**, 1239–1254.

Fichman, G., Guterman, T., Damron, J., Adler-Abramovich, L., Schmidt, J., Kesselman, E., Shimon, L. J. W., Ramamoorthy, A., Talmon, Y. & Gazit, E. (2016). *Sci. Adv.* **2**, e1500827.

Fleming, S. & Ulijn, R. V. (2014). *Chem. Soc. Rev.* **43**, 8150–8177.

Frisch, M. J., *et al.* (2011). *GAUSSIAN09*. Version 9.0. Gaussian Inc., Wallingford, CT, USA. https://gaussian.com/gaussian16/.

Ganguly, P. & Desiraju, G. R. (2010). *CrystEngComm*, **12**, 817–833.

Gonzalez, J., Ramirez, J. & Schwans, J. P. (2016). *Amino Acids*, **48**, 2755–2763.

Groom, C. R., Bruno, I. J., Lightfoot, M. P. & Ward, S. C. (2016). *Acta Cryst.* B**72**, 171–179.

Guidotti, G., Brambilla, L. & Rossi, D. (2017). *Trends Pharmacol. Sci.* **38**, 406–424.

Hammarstrom, L. G. J., McLaughlin, M. L. & Fronczek, F. R. (2013). Private Communication (refcode CUWKOU01). CCDC, Cambridge, England.

Henninot, A., Collins, J. C. & Nuss, J. M. (2018). *J. Med. Chem.* **61**, 1382–1414.

Ikeda, M., Tanida, T., Yoshii, T., Kurotani, K., Onogi, S., Urayama, K. & Hamachi, I. (2014). *Nat. Chem.* **6**, 511–518.

Jayatilaka, D. & Grimwood, D. J. (2003). *Comput. Sci.* **4**, 142–151.

Jayawarna, V., Richardson, S. M., Hirst, A. R., Hodson, N. W., Saiani, A., Gough, J. E. & Ulijn, R. V. (2009). *Acta Biomater.* **5**, 934–943.

Kasim, J. K., Kavianinia, I., Harris, P. R. W. & Brimble, M. A. (2019). *Frontiers Chem.* **7**, 1–25.

Khavinson, V., Linkova, N. S., Kukanova, E. O., Bolshakova, A. V., Gainullina, A. N., Tendler, S. M., Morozova, E., Tarnovskaya, S., Pada Vinski, D. S. & Nina Kasyanenko, V. B. (2017). *J. Neurol. Neurosci.* **08**, 166.

Kitaigorodskii, A. I. (1961). *Organic Chemical Crystallography*, pp. 1–30, 65–112. New York: Consultants Bureau.

Kitaigorodskii, A. I. (1973). *Molecular Crystals and Molecules*, pp. 1–133. London: Academic Press.

Klamt, A. & Schüürmann, G. (1993). *J. Chem. Soc. Perkin Trans. 2*, pp. 799–805.

Kraskovskaya, N. A., Kukanova, E. O., Lin'kova, N. S., Popugaeva, E. A. & Khavinson, V. K. (2017). *Bull. Exp. Biol. Med.* **163**, 550–553.

Lee, A. C. L., Harris, J. L., Khanna, K. K. & Hong, J. H. (2019). *Int. J. Mol. Sci.* **20**, 2383–2404.

Lee, C., Yang, W. & Parr, R. G. (1988). *Phys. Rev. B*, **37**, 785–789.

Liang, G., Yang, Z., Zhang, R., Li, L., Fan, Y., Kuang, Y., Gao, Y., Wang, T., Lu, W. W. & Xu, B. (2009). *Langmuir*, **25**, 8419–8422.

Liebmann, T., Rydholm, S., Akpe, V. & Brismar, H. (2007). *BMC Biotechnol.* **7**, 88.

Liu, J. F., Tang, X. X. & Jiang, B. (2002). *Synthesis*, pp. 1499–1501.

Liyanage, W. & Nilsson, B. L. (2016). *Langmuir*, **32**, 787–799.

Loots, L. & Barbour, L. J. (2012). *CrystEngComm*, **14**, 300–304.

Macrae, C. F., Sovago, I., Cottrell, S. J., Galek, P. T. A., McCabe, P., Pidcock, E., Platings, M., Shields, G. P., Stevens, J. S., Towler, M. & Wood, P. A. (2020). *J. Appl. Cryst.* **53**, 226–235.

Mahler, A., Reches, M., Rechter, M., Cohen, S. & Gazit, E. (2006). *Adv. Mater.* **18**, 1365–1370.

Mazur, L., Koziol, A. E., Rzeszotarska, B. & Masiukiewicz, E. (2002). *Lett. Pept. Sci.* **9**, 697–712.

McKinnon, J. J., Jayatilaka, D. & Spackman, M. A. (2007). *Chem. Commun.* pp. 3814–3816.

McKinnon, J. J., Mitchell, A. S. & Spackman, M. A. (1998). *Chem. Eur. J.* **4**, 2136–2141.

Meyer, A. Y. (1986). *Chem. Soc. Rev.* **15**, 449–474.

Nalluri, S. K. M., Shivarova, N., Kanibolotsky, A. L., Zelzer, M., Gupta, S., Frederix, P. W. J. M., Skabara, P. J., Gleskova, H. & Ulijn, R. V. (2014). *Langmuir*, **30**, 12429–12437.

Neumann, R., Nobes, R. H. & Handy, N. C. (1996). *Mol. Phys.* **87**, 1–36.

Nielsen, A. B. & Holder, A. J. (2009). *GaussView*. Gaussian Inc., Pittsburgh, USA. https://gaussian.com/gaussview6/.

Pai, V. V., Bhandari, P. & Shukla, P. (2017). *Indian J. Dermatol. Venereol. Leprol.* **83**, 9–18.

Palaninathan, S. K., Mohamedmohaideen, N. N., Orlandini, E., Ortore, G., Nencetti, S., Lapucci, A., Rossello, A., Freundlich, J. S. & Sacchettini, J. C. (2009). *PLoS One*, **4**, e6290.

Parr, R. G. & Wang, W. (1994). In *Density-Functional Theory of Atoms and Molecules*. New York: Oxford University Press.

Parsons, S. & Flack, H. (2004). *Acta Cryst.* A**60**, s61.

Pingul, B. Y., Ramirez, J. & Schwans, J. (2019). *FASEB J.* **33**, Abstract No. 470.12.

Pizzi, A., Lascialfari, L., Demitri, N., Bertolani, A., Maiolo, D., Carretti, A. & Metrangolo, P. (2017). *CrystEngComm*, **19**, 1870–1874.

Raeburn, J., Mendoza-Cuenca, C., Cattoz, B. N., Little, M. A., Terry, A. E., Zamith Cardoso, A., Griffiths, P. C. & Adams, D. J. (2015). *Soft Matter*, **11**, 927–935.
Rajbhandary, A., Brennessel, W. W. & Nilsson, B. L. (2018). *Cryst. Growth Des.* **18**, 623–632.
Ramirez, J., Gonzales, J. & Schwans, J. (2018). *FASEB J.* **32**, Abstract No. 797.7.
Rohl, A. L., Moret, M., Kaminsky, W., Claborn, K., McKinnon, J. J. & Kahr, B. (2008). *Cryst. Growth Des.* **8**, 4517–4525.
Rudat, B., Birtalan, E., Vollrath, S. B. L., Fritz, D., Kölmel, K., Nieger, M., Schepers, U., Müllen, K., Eisler, H. J., Lemmer, U. & Bräse, S. (2011). *Eur. J. Med. Chem.* **46**, 4457–4465.
Rudnick, J. & Gaspari, G. (1986). *J. Phys. A Math. Gen.* **19**, L191–L193.
Ryan, D. M. & Nilsson, B. L. (2012). *Polym. Chem.* **3**, 18–33.
Sánchez, A. & Vázquez, A. (2017). *Food. Qual. Saf.* **1**, 29–46.
Scroggs, A., Hammer, R. P. & Fronczek, F. R. (2015). Private Communication (refcode MOXSUP). CCDC, Cambridge, England.
Sheldrick, G. M. (2008). *SADABS*. University of Göttingen, Germany.
Sheldrick, G. M. (2015*a*). *Acta Cryst.* A**71**, 3–8.
Sheldrick, G. M. (2015*b*). *Acta Cryst.* C**71**, 3–8.
Siemens (1996). *XSCANS*. Siemens Analytical X-ray Instruments Inc., Madison, Wisconsin, USA.
Silva, C. S., Eira, J., Ribeiro, C. A., Oliveira, A., Sousa, M. M., Cardoso, I. & Liz, M. A. (2017). *Neurobiol. Aging*, **59**, 10–14.
Spackman, M. A. & Jayatilaka, D. (2009). *CrystEngComm* **11**, 19–32.
Spackman, M. A. & Byrom, P. G. (1997). *Chem. Phys. Lett.* **267**, 215–220.
Spackman, M. A. & McKinnon, J. J. (2002). *CrystEngComm*, **4**, 378–392.
Spackman, M. A., McKinnon, J. J. & Jayatilaka, D. (2008). *CrystEngComm*, **10**, 377–388.
Spek, A. L. (2020). *Acta Cryst.* E**76**, 1–11.
Stefanowicz, P., Jaremko, L., Jaremko, M., Staszewska, A., Szewczuk, Z., Bryndal, I. & Lis, T. (2006). *Acta Cryst.* E**62**, o3555–o3557.
Steiner, T. (2002). *Angew. Chem. Int. Ed.* **41**, 48–76.
Sutton, S., Campbell, N. L., Cooper, A. I., Kirkland, M., Frith, W. J. & Adams, D. A. (2009). *Langmuir*, **25**, 10285–10291.
Turner, M. J., McKinnon, J. J., Wolff, S. K., Grimwood, D. J., Spackman, P. R., Jayatilaka, D. & Spackman, M. A. (2017). *CrystalExplorer17.5*. University of Western Australia, Perth, Australia. http://crystalexplorer.scb.uwa.edu.au/.
Venkatesan, P., Thamotharan, S., Ilangovan, A., Liang, H. & Sundius, T. (2016). *Spectrochim. Acta A Mol. Biomol. Spectrosc.* **153**, 625–636.
Wang, J., Hammer, R. P. & Fronczek, F. R. (2015). Private Communication (refcode DULLAZ). CCDC, Cambridge, England.
Wolff, S. K., Grimwood, D. J., McKinnon, J. J., Jayatilaka, D. & Spackman, M. A. (2012). *CrystalExplorer3.1*. The University of Western Australia. http://crystalexplorer.scb.uwa.edu.au/.
Wood, P. A., Olsson, T. S. G., Cole, J. C., Cottrell, S. J., Feeder, N., Galek, P. T. A., Groom, C. R. & Pidcock, E. (2013). *CrystEngComm*, **15**, 65–72.
World Health Organization (2019). *Dementia*. Available online at: https://www.who.int/news-room/fact-sheets/detail/dementia (accessed February 25, 2019).
Wu, H., Qiao, Q., Hu, Y., Teng, P., Gao, W., Zuo, X., Wojtas, L., Larsen, R. W., Ma, S. & Cai, J. (2015). *Chem. Eur. J.* **21**, 2501–2507.
Xing, P., Li, P., Chen, H., Hao, A. & Zhao, Y. (2017). *ACS Nano*, **11**, 4206–4216.
Yamada, K., Hashizume, D., Shimizu, T. & Deguchi, K. (2008). *Acta Cryst.* E**64**, o1533.
Young, T. & Kiessling, L. L. (2002). *Angew. Chem. Int. Ed.* **41**, 3449–3451.
Zamorskii, I. I., Shchudrova, T. S., Lin'kova, N. S., Nichik, T. E. & Khavinson, V. K. (2017). *Bull. Exp. Biol. Med.* **163**, 389–393.
Zhou, J., Li, J., Du, X. & Xu, B. (2017). *Biomaterials*, **129**, 1–27.

supporting information

Acta Cryst. (2020). C**76**, 328-345 [https://doi.org/10.1107/S2053229620003009]

Synthesis, experimental and *in silico* studies of *N*-fluorenylmethoxycarbonyl-*O*-*tert*-butyl-*N*-methyltyrosine, coupled with CSD data: a survey of interactions in the crystal structures of Fmoc–amino acids

Joanna Bojarska, Milan Remko, Izabela D. Madura, Krzysztof Kaczmarek, Janusz Zabrocki and Wojciech M. Wolf

Computing details

Data collection: *XSCANS* (Siemens, 1996); cell refinement: *XSCANS* (Siemens, 1996); data reduction: *XSCANS* (Siemens, 1996); program(s) used to solve structure: SHELXT (Sheldrick, 2015a); program(s) used to refine structure: *SHELXL2014* (Sheldrick, 2015b); software used to prepare material for publication: *SHELXL2014* (Sheldrick, 2015b).

2-{[(9*H*-Fluoren-9-ylmethoxy)carbonyl](methyl)amino}-3-{4-[(2-hydroxypropan-2-yl)oxy]phenyl}propanoic acid

Crystal data

$C_{29}H_{31}NO_5$
M_r = 473.55
Orthorhombic, $P2_12_12_1$
a = 6.4917 (3) Å
b = 17.5357 (7) Å
c = 22.2418 (8) Å
V = 2531.93 (18) Å^3
Z = 4
$F(000)$ = 1008
D_x = 1.242 Mg m^{-3}
Mo $K\alpha$ radiation, λ = 0.71073 Å
Cell parameters from 9925 reflections
θ = 2.3–28.6°
μ = 0.09 mm^{-1}
T = 296 K
Plate, colourless
0.60 × 0.25 × 0.15 mm

Data collection

Siemens P3 diffractometer
Radiation source: fine-focus sealed tube
profile data from $\theta/2\theta$ scans
Absorption correction: multi-scan (SADABS; Sheldrick, 2008)
T_{min} = 0.872, T_{max} = 0.992
58330 measured reflections
5823 independent reflections
5543 reflections with $I > 2\sigma(I)$
R_{int} = 0.022
θ_{max} = 27.5°, θ_{min} = 1.5°
h = −8→8
k = −22→22
l = −28→28

Refinement

Refinement on F^2
Least-squares matrix: full
$R[F^2 > 2\sigma(F^2)]$ = 0.032
$wR(F^2)$ = 0.091
S = 0.99
5823 reflections
396 parameters
0 restraints
Primary atom site location: structure-invariant direct methods
Secondary atom site location: difference Fourier map
Hydrogen site location: mixed
H atoms treated by a mixture of independent and constrained refinement

$w = 1/[\sigma^2(F_o^2) + (0.0623P)^2 + 0.2078P]$
where $P = (F_o^2 + 2F_c^2)/3$
$(\Delta/\sigma)_{max} = 0.001$
$\Delta\rho_{max} = 0.15$ e Å^{-3}
$\Delta\rho_{min} = -0.16$ e Å^{-3}

Absolute structure: Flack *x* determined using 2313 quotients [(I+)-(I-)]/[(I+)+(I-)] (Parsons & Flack, 2004)
Absolute structure parameter: 0.19 (14)

Special details

Geometry. All esds (except the esd in the dihedral angle between two l.s. planes) are estimated using the full covariance matrix. The cell esds are taken into account individually in the estimation of esds in distances, angles and torsion angles; correlations between esds in cell parameters are only used when they are defined by crystal symmetry. An approximate (isotropic) treatment of cell esds is used for estimating esds involving l.s. planes.

Refinement. The SC-XRD was performed on a Siemens P3 diffractometer using graphite monochromated Mo *Kα* radiation (λ = 0.71073 Å) as a source of radiation. The structure was solved with the SHELXS structure solution program and refined in the SHELXL-2014 (Sheldrick, 2015) by the full-matrix least-squares on F^2. All non-hydrogen atoms were initially located on *E* maps and refined anisotropically.

Fractional atomic coordinates and isotropic or equivalent isotropic displacement parameters (Å²)

	x	*y*	*z*	U_{iso}*/U_{eq}
N1	0.40982 (19)	−0.08075 (7)	0.97111 (6)	0.0360 (3)
O3	0.5064 (2)	−0.27780 (7)	0.93447 (6)	0.0530 (3)
O1	−0.0581 (2)	0.08123 (8)	0.76045 (5)	0.0557 (3)
O2	0.5219 (3)	−0.21723 (7)	1.02265 (6)	0.0582 (4)
C23	−0.2349 (3)	0.16051 (8)	1.02378 (8)	0.0395 (3)
C14	0.2537 (2)	−0.05737 (8)	1.00620 (7)	0.0346 (3)
O4	0.08814 (18)	−0.09013 (6)	1.01111 (6)	0.0467 (3)
C13	0.4813 (3)	−0.21821 (8)	0.97018 (7)	0.0394 (3)
C16	0.0909 (3)	0.11810 (9)	1.06152 (7)	0.0396 (3)
C11	0.4532 (3)	−0.14247 (10)	0.87096 (8)	0.0448 (4)
O5	0.29769 (19)	0.00778 (7)	1.03506 (6)	0.0458 (3)
C28	−0.0475 (3)	0.12640 (8)	1.00715 (7)	0.0394 (3)
C22	−0.2289 (3)	0.17649 (8)	1.08842 (8)	0.0405 (3)
C8	0.3252 (3)	−0.08382 (9)	0.83773 (7)	0.0432 (3)
C12	0.3838 (2)	−0.15093 (8)	0.93673 (7)	0.0362 (3)
C24	−0.3857 (3)	0.17599 (9)	0.98133 (8)	0.0470 (4)
C17	−0.0380 (3)	0.15294 (9)	1.11122 (7)	0.0419 (3)
C27	−0.0115 (3)	0.10738 (10)	0.94742 (8)	0.0489 (4)
C15	0.1475 (3)	0.03615 (10)	1.07729 (8)	0.0468 (4)
C1	−0.0793 (3)	0.09457 (12)	0.69571 (7)	0.0531 (4)
C19	−0.1362 (5)	0.19791 (14)	1.20822 (9)	0.0687 (6)
C25	−0.3483 (4)	0.15657 (11)	0.92150 (9)	0.0552 (4)
C5	0.0729 (3)	0.02494 (10)	0.78133 (7)	0.0457 (4)
C18	0.0089 (4)	0.16336 (12)	1.17156 (9)	0.0567 (5)
C7	0.1252 (4)	−0.10153 (12)	0.81968 (10)	0.0582 (5)
C26	−0.1640 (4)	0.12277 (11)	0.90508 (9)	0.0567 (5)
C29	0.6171 (3)	−0.04817 (11)	0.97609 (9)	0.0491 (4)
H29A	0.6116	−0.0022	0.9995	0.059*
H29B	0.6688	−0.0367	0.9367	0.059*
H29C	0.7068	−0.0842	0.9953	0.059*

C10	0.2722 (3)	0.04351 (11)	0.79854 (9)	0.0544 (4)
C9	0.3956 (3)	−0.01074 (12)	0.82630 (9)	0.0532 (4)
C6	0.0011 (3)	−0.04802 (13)	0.79183 (10)	0.0600 (5)
C21	−0.3733 (3)	0.21104 (11)	1.12580 (9)	0.0546 (4)
C20	−0.3228 (4)	0.22187 (14)	1.18594 (10)	0.0688 (6)
C2	0.1203 (5)	0.12258 (15)	0.66979 (10)	0.0692 (6)
H2A	0.1643	0.1672	0.6912	0.083*
H2B	0.1012	0.1349	0.6281	0.083*
H2C	0.2230	0.0835	0.6735	0.083*
C3	−0.1507 (5)	0.02203 (17)	0.66476 (11)	0.0802 (8)
H3A	−0.0515	−0.0177	0.6714	0.096*
H3B	−0.1644	0.0312	0.6224	0.096*
H3C	−0.2815	0.0068	0.6809	0.096*
C4	−0.2427 (5)	0.15678 (19)	0.69363 (14)	0.0886 (9)
H4A	−0.3668	0.1386	0.7122	0.106*
H4B	−0.2705	0.1700	0.6525	0.106*
H4C	−0.1939	0.2009	0.7148	0.106*
H121	0.236 (3)	−0.1625 (11)	0.9379 (8)	0.037 (5)*
H271	0.112 (4)	0.0871 (13)	0.9356 (10)	0.057 (6)*
H112	0.605 (4)	−0.1285 (12)	0.8696 (9)	0.049 (5)*
H91	0.530 (4)	0.0020 (15)	0.8349 (12)	0.069 (7)*
H151	0.032 (4)	0.0014 (12)	1.0755 (10)	0.048 (5)*
H241	−0.515 (4)	0.2013 (14)	0.9950 (10)	0.061 (6)*
H111	0.436 (4)	−0.1907 (14)	0.8531 (10)	0.059 (6)*
H181	0.137 (4)	0.1454 (15)	1.1878 (11)	0.066 (7)*
H161	0.217 (4)	0.1451 (13)	1.0553 (10)	0.053 (6)*
H61	−0.144 (4)	−0.0624 (14)	0.7784 (10)	0.063 (6)*
H101	0.325 (3)	0.0959 (13)	0.7930 (9)	0.052 (5)*
H201	−0.413 (6)	0.2460 (19)	1.2134 (15)	0.099 (10)*
H71	0.070 (4)	−0.1525 (17)	0.8276 (11)	0.072 (7)*
H221	−0.504 (4)	0.2285 (15)	1.1090 (11)	0.061 (6)*
H251	−0.459 (5)	0.1670 (15)	0.8923 (12)	0.073 (8)*
H3	0.538 (5)	−0.3189 (16)	0.9576 (12)	0.074 (7)*
H152	0.213 (4)	0.0359 (14)	1.1168 (12)	0.062 (6)*
H261	−0.137 (4)	0.1106 (15)	0.8636 (12)	0.072 (7)*
H191	−0.100 (5)	0.2089 (18)	1.2504 (15)	0.098 (10)*

Atomic displacement parameters (Å²)

	U^{11}	U^{22}	U^{33}	U^{12}	U^{13}	U^{23}
N1	0.0294 (6)	0.0317 (6)	0.0468 (6)	0.0017 (5)	0.0004 (5)	−0.0009 (5)
O3	0.0721 (9)	0.0368 (5)	0.0502 (6)	0.0172 (6)	−0.0111 (6)	−0.0032 (5)
O1	0.0680 (8)	0.0635 (7)	0.0356 (5)	0.0254 (7)	−0.0058 (5)	0.0024 (5)
O2	0.0841 (10)	0.0466 (6)	0.0439 (6)	0.0179 (7)	−0.0119 (7)	0.0006 (5)
C23	0.0441 (8)	0.0294 (6)	0.0449 (8)	−0.0015 (6)	0.0049 (6)	−0.0002 (6)
C14	0.0313 (7)	0.0278 (6)	0.0448 (7)	0.0040 (5)	−0.0005 (6)	0.0067 (5)
O4	0.0342 (5)	0.0373 (5)	0.0686 (7)	−0.0021 (4)	0.0076 (5)	0.0011 (5)
C13	0.0417 (8)	0.0340 (6)	0.0425 (7)	0.0059 (6)	−0.0032 (6)	0.0012 (6)

C16	0.0388 (8)	0.0335 (7)	0.0464 (8)	0.0005 (6)	0.0046 (6)	−0.0029 (6)
C11	0.0506 (10)	0.0419 (8)	0.0419 (8)	0.0100 (7)	0.0004 (7)	0.0013 (6)
O5	0.0390 (6)	0.0380 (5)	0.0605 (7)	0.0006 (5)	0.0078 (5)	−0.0096 (5)
C28	0.0433 (8)	0.0304 (6)	0.0444 (8)	−0.0020 (6)	0.0061 (6)	0.0005 (5)
C22	0.0459 (8)	0.0302 (6)	0.0454 (8)	0.0006 (6)	0.0055 (7)	−0.0017 (6)
C8	0.0486 (9)	0.0433 (8)	0.0376 (7)	0.0050 (7)	−0.0035 (7)	0.0026 (6)
C12	0.0349 (7)	0.0324 (6)	0.0412 (7)	0.0043 (6)	−0.0028 (6)	0.0006 (5)
C24	0.0481 (9)	0.0381 (7)	0.0549 (9)	0.0011 (7)	−0.0003 (8)	0.0037 (7)
C17	0.0488 (9)	0.0323 (7)	0.0447 (8)	0.0018 (6)	0.0039 (7)	−0.0036 (6)
C27	0.0574 (10)	0.0438 (8)	0.0454 (8)	0.0010 (8)	0.0124 (8)	−0.0013 (6)
C15	0.0494 (9)	0.0402 (8)	0.0509 (9)	0.0105 (7)	0.0086 (8)	0.0002 (7)
C1	0.0621 (11)	0.0608 (10)	0.0363 (7)	0.0069 (9)	−0.0128 (8)	0.0042 (7)
C19	0.0937 (18)	0.0685 (13)	0.0439 (9)	0.0093 (13)	0.0037 (11)	−0.0132 (9)
C25	0.0682 (12)	0.0461 (9)	0.0513 (9)	−0.0037 (9)	−0.0101 (9)	0.0058 (7)
C5	0.0524 (10)	0.0495 (8)	0.0351 (7)	0.0127 (7)	−0.0052 (7)	0.0010 (6)
C18	0.0691 (13)	0.0530 (10)	0.0480 (9)	0.0055 (10)	−0.0070 (9)	−0.0065 (8)
C7	0.0569 (11)	0.0495 (10)	0.0682 (12)	−0.0057 (9)	−0.0133 (10)	0.0100 (8)
C26	0.0791 (14)	0.0488 (9)	0.0422 (8)	−0.0048 (9)	0.0049 (9)	0.0005 (7)
C29	0.0318 (7)	0.0515 (9)	0.0641 (10)	−0.0046 (7)	0.0042 (8)	−0.0090 (8)
C10	0.0630 (11)	0.0447 (9)	0.0553 (10)	−0.0026 (8)	−0.0147 (9)	0.0087 (8)
C9	0.0504 (10)	0.0517 (9)	0.0575 (10)	−0.0046 (8)	−0.0151 (8)	0.0100 (8)
C6	0.0485 (10)	0.0665 (12)	0.0650 (12)	−0.0031 (9)	−0.0129 (9)	0.0096 (9)
C21	0.0549 (11)	0.0488 (9)	0.0600 (10)	0.0107 (8)	0.0113 (9)	−0.0075 (8)
C20	0.0808 (15)	0.0682 (13)	0.0574 (11)	0.0162 (12)	0.0198 (11)	−0.0164 (10)
C2	0.0872 (16)	0.0677 (12)	0.0526 (10)	−0.0089 (13)	−0.0005 (11)	0.0016 (10)
C3	0.097 (2)	0.0905 (17)	0.0535 (11)	−0.0239 (16)	−0.0172 (13)	−0.0050 (11)
C4	0.0912 (19)	0.0972 (19)	0.0773 (16)	0.0346 (16)	−0.0253 (15)	0.0161 (14)

Geometric parameters (Å, º)

N1—C14	1.3434 (19)	C15—H152	0.98 (3)
N1—C12	1.4587 (19)	C1—C2	1.501 (3)
N1—C29	1.466 (2)	C1—C3	1.519 (3)
O3—C13	1.3226 (19)	C1—C4	1.522 (3)
O3—H3	0.91 (3)	C19—C20	1.375 (4)
O1—C5	1.383 (2)	C19—C18	1.385 (3)
O1—C1	1.465 (2)	C19—H191	0.99 (3)
O2—C13	1.197 (2)	C25—C26	1.384 (3)
C23—C24	1.387 (3)	C25—H251	0.99 (3)
C23—C28	1.406 (2)	C5—C6	1.382 (3)
C23—C22	1.465 (2)	C5—C10	1.388 (3)
C14—O4	1.2233 (19)	C18—H181	0.96 (3)
C14—O5	1.3413 (19)	C7—C6	1.383 (3)
C13—C12	1.532 (2)	C7—H71	0.98 (3)
C16—C28	1.513 (2)	C26—H261	0.96 (3)
C16—C17	1.515 (2)	C29—H29A	0.9600
C16—C15	1.524 (2)	C29—H29B	0.9600
C16—H161	0.95 (2)	C29—H29C	0.9600

C11—C8	1.515 (2)	C10—C9	1.389 (3)
C11—C12	1.538 (2)	C10—H101	0.99 (2)
C11—H112	1.02 (2)	C9—H91	0.92 (3)
C11—H111	0.94 (3)	C6—H61	1.02 (3)
O5—C15	1.442 (2)	C21—C20	1.390 (3)
C28—C27	1.389 (2)	C21—H221	0.98 (3)
C22—C21	1.392 (2)	C20—H201	0.95 (4)
C22—C17	1.401 (2)	C2—H2A	0.9600
C8—C9	1.384 (3)	C2—H2B	0.9600
C8—C7	1.394 (3)	C2—H2C	0.9600
C12—H121	0.98 (2)	C3—H3A	0.9600
C24—C25	1.395 (3)	C3—H3B	0.9600
C24—H241	1.00 (3)	C3—H3C	0.9600
C17—C18	1.388 (3)	C4—H4A	0.9600
C27—C26	1.393 (3)	C4—H4B	0.9600
C27—H271	0.91 (3)	C4—H4C	0.9600
C15—H151	0.97 (2)		

C14—N1—C12	118.33 (13)	O1—C1—C4	102.11 (18)
C14—N1—C29	122.00 (13)	C2—C1—C4	110.8 (2)
C12—N1—C29	118.33 (13)	C3—C1—C4	111.9 (2)
C13—O3—H3	108.2 (16)	C20—C19—C18	121.4 (2)
C5—O1—C1	120.11 (14)	C20—C19—H191	119 (2)
C24—C23—C28	121.01 (16)	C18—C19—H191	119 (2)
C24—C23—C22	130.50 (16)	C26—C25—C24	120.45 (19)
C28—C23—C22	108.45 (15)	C26—C25—H251	122.4 (16)
O4—C14—O5	122.98 (14)	C24—C25—H251	117.1 (16)
O4—C14—N1	124.85 (14)	C6—C5—O1	120.67 (18)
O5—C14—N1	112.16 (13)	C6—C5—C10	119.03 (17)
O2—C13—O3	124.75 (15)	O1—C5—C10	119.89 (17)
O2—C13—C12	123.62 (14)	C19—C18—C17	118.5 (2)
O3—C13—C12	111.57 (13)	C19—C18—H181	120.7 (15)
C28—C16—C17	102.50 (13)	C17—C18—H181	120.8 (15)
C28—C16—C15	114.68 (14)	C6—C7—C8	121.37 (19)
C17—C16—C15	110.19 (14)	C6—C7—H71	119.3 (16)
C28—C16—H161	110.1 (14)	C8—C7—H71	119.3 (16)
C17—C16—H161	112.2 (14)	C25—C26—C27	121.28 (18)
C15—C16—H161	107.2 (14)	C25—C26—H261	120.5 (17)
C8—C11—C12	111.64 (14)	C27—C26—H261	118.2 (17)
C8—C11—H112	110.8 (12)	N1—C29—H29A	109.5
C12—C11—H112	109.6 (12)	N1—C29—H29B	109.5
C8—C11—H111	109.8 (14)	H29A—C29—H29B	109.5
C12—C11—H111	106.3 (14)	N1—C29—H29C	109.5
H112—C11—H111	108.5 (19)	H29A—C29—H29C	109.5
C14—O5—C15	117.48 (13)	H29B—C29—H29C	109.5
C27—C28—C23	119.95 (17)	C5—C10—C9	119.99 (19)
C27—C28—C16	129.87 (16)	C5—C10—H101	120.4 (13)
C23—C28—C16	110.15 (14)	C9—C10—H101	119.6 (13)

C21—C22—C17	120.51 (17)	C8—C9—C10	121.68 (19)
C21—C22—C23	130.65 (18)	C8—C9—H91	120.0 (17)
C17—C22—C23	108.81 (14)	C10—C9—H91	118.2 (17)
C9—C8—C7	117.46 (16)	C5—C6—C7	120.47 (19)
C9—C8—C11	122.45 (17)	C5—C6—H61	119.5 (14)
C7—C8—C11	120.03 (16)	C7—C6—H61	120.0 (14)
N1—C12—C13	110.33 (12)	C20—C21—C22	118.4 (2)
N1—C12—C11	112.54 (13)	C20—C21—H221	122.0 (15)
C13—C12—C11	114.53 (13)	C22—C21—H221	119.6 (15)
N1—C12—H121	105.9 (11)	C19—C20—C21	120.8 (2)
C13—C12—H121	103.5 (11)	C19—C20—H201	117 (2)
C11—C12—H121	109.3 (11)	C21—C20—H201	122 (2)
C23—C24—C25	118.60 (18)	C1—C2—H2A	109.5
C23—C24—H241	118.3 (13)	C1—C2—H2B	109.5
C25—C24—H241	123.1 (13)	H2A—C2—H2B	109.5
C18—C17—C22	120.34 (17)	C1—C2—H2C	109.5
C18—C17—C16	129.59 (18)	H2A—C2—H2C	109.5
C22—C17—C16	110.07 (14)	H2B—C2—H2C	109.5
C28—C27—C26	118.70 (18)	C1—C3—H3A	109.5
C28—C27—H271	121.0 (14)	C1—C3—H3B	109.5
C26—C27—H271	120.2 (14)	H3A—C3—H3B	109.5
O5—C15—C16	109.77 (14)	C1—C3—H3C	109.5
O5—C15—H151	106.2 (13)	H3A—C3—H3C	109.5
C16—C15—H151	113.5 (13)	H3B—C3—H3C	109.5
O5—C15—H152	106.9 (15)	C1—C4—H4A	109.5
C16—C15—H152	108.4 (15)	C1—C4—H4B	109.5
H151—C15—H152	112 (2)	H4A—C4—H4B	109.5
O1—C1—C2	110.38 (17)	C1—C4—H4C	109.5
O1—C1—C3	109.91 (17)	H4A—C4—H4C	109.5
C2—C1—C3	111.3 (2)	H4B—C4—H4C	109.5

C12—N1—C14—O4	−1.0 (2)	C23—C22—C17—C16	−1.21 (18)
C29—N1—C14—O4	−167.57 (16)	C28—C16—C17—C18	−178.38 (18)
C12—N1—C14—O5	−179.84 (12)	C15—C16—C17—C18	59.1 (2)
C29—N1—C14—O5	13.6 (2)	C28—C16—C17—C22	1.36 (17)
O4—C14—O5—C15	5.2 (2)	C15—C16—C17—C22	−121.14 (16)
N1—C14—O5—C15	−175.97 (14)	C23—C28—C27—C26	0.0 (2)
C24—C23—C28—C27	−0.3 (2)	C16—C28—C27—C26	−178.33 (16)
C22—C23—C28—C27	−178.23 (15)	C14—O5—C15—C16	−125.56 (16)
C24—C23—C28—C16	178.33 (14)	C28—C16—C15—O5	74.60 (19)
C22—C23—C28—C16	0.37 (17)	C17—C16—C15—O5	−170.39 (15)
C17—C16—C28—C27	177.39 (16)	C5—O1—C1—C2	−65.0 (2)
C15—C16—C28—C27	−63.2 (2)	C5—O1—C1—C3	58.2 (3)
C17—C16—C28—C23	−1.03 (16)	C5—O1—C1—C4	177.2 (2)
C15—C16—C28—C23	118.37 (15)	C23—C24—C25—C26	−0.2 (3)
C24—C23—C22—C21	0.7 (3)	C1—O1—C5—C6	−92.0 (2)
C28—C23—C22—C21	178.41 (18)	C1—O1—C5—C10	95.5 (2)
C24—C23—C22—C17	−177.17 (16)	C20—C19—C18—C17	−0.2 (4)

C28—C23—C22—C17	0.53 (17)	C22—C17—C18—C19	−0.5 (3)
C12—C11—C8—C9	102.0 (2)	C16—C17—C18—C19	179.24 (19)
C12—C11—C8—C7	−75.2 (2)	C9—C8—C7—C6	−0.5 (3)
C14—N1—C12—C13	−96.94 (16)	C11—C8—C7—C6	176.9 (2)
C29—N1—C12—C13	70.12 (18)	C24—C25—C26—C27	−0.1 (3)
C14—N1—C12—C11	133.77 (15)	C28—C27—C26—C25	0.2 (3)
C29—N1—C12—C11	−59.17 (19)	C6—C5—C10—C9	−0.5 (3)
O2—C13—C12—N1	18.3 (2)	O1—C5—C10—C9	172.13 (18)
O3—C13—C12—N1	−164.27 (14)	C7—C8—C9—C10	0.7 (3)
O2—C13—C12—C11	146.51 (19)	C11—C8—C9—C10	−176.61 (19)
O3—C13—C12—C11	−36.1 (2)	C5—C10—C9—C8	−0.2 (3)
C8—C11—C12—N1	−62.63 (18)	O1—C5—C6—C7	−171.88 (19)
C8—C11—C12—C13	170.29 (14)	C10—C5—C6—C7	0.7 (3)
C28—C23—C24—C25	0.4 (2)	C8—C7—C6—C5	−0.2 (3)
C22—C23—C24—C25	177.83 (17)	C17—C22—C21—C20	0.3 (3)
C21—C22—C17—C18	0.4 (3)	C23—C22—C21—C20	−177.3 (2)
C23—C22—C17—C18	178.56 (16)	C18—C19—C20—C21	1.0 (4)
C21—C22—C17—C16	−179.35 (16)	C22—C21—C20—C19	−1.0 (4)

Hydrogen-bond geometry (Å, º)

D—H···*A*	*D*—H	H···*A*	*D*···*A*	*D*—H···*A*
O3—H3···O4^{i}	0.91	1.77	2.666 (1)	168
C29—H29*C*···O4^{ii}	0.96	2.50	3.240 (2)	134
C15—H151···O4	0.97	2.18	2.687 (2)	111
C26—H261···O1	0.96	2.41	3.369 (2)	178

Symmetry codes: (i) *x*+1/2, −*y*−1/2, −*z*+2; (ii) *x*+1, *y*, *z*.